



Published in final edited form as:

Sci Signal. ; 8(395): ra95. doi:10.1126/scisignal.aaa6179.

## Dichotomous roles for externalized cardiolipin in extracellular signaling: Promotion of phagocytosis and attenuation of innate immunity

Krishnakumar Balasubramanian<sup>1,\*</sup>, Akihiro Maeda<sup>2</sup>, Janet S. Lee<sup>3</sup>, Dariush Mohammadyani<sup>1</sup>, Haider Hussain Dar<sup>1</sup>, Jian Fei Jiang<sup>1</sup>, Claudette M. St. Croix<sup>4</sup>, Simon Watkins<sup>4</sup>, Vladimir A. Tyurin<sup>1</sup>, Yulia Y. Tyurina<sup>1</sup>, Katharina Klöditz<sup>2</sup>, Anastassia Polimova<sup>1</sup>, Valentyna I. Kapralova<sup>1</sup>, Zeyu Xiong<sup>3</sup>, Prabir Ray<sup>3</sup>, Judith Klein-Seetharaman<sup>5</sup>, Rama K. Mallampalli<sup>6,7</sup>, Hülya Bayir<sup>1,8</sup>, Bengt Fadeel<sup>2,\*</sup>, and Valerian E. Kagan<sup>1,\*</sup>

<sup>1</sup>Center for Free Radical and Antioxidant Health, Department of Environmental and Occupational Health, University of Pittsburgh, Pittsburgh, PA 15219, USA

<sup>2</sup>Division of Molecular Toxicology, Institute of Environmental Medicine, Karolinska Institutet, Stockholm 171 77, Sweden

<sup>3</sup>Division of Pulmonary, Allergy and Critical Care Medicine, Department of Medicine, University of Pittsburgh School of Medicine, Pittsburgh, PA 15213, USA

**Permissions** Obtain information about reproducing this article: <http://www.sciencemag.org/about/permissions.dtl>

\*Corresponding author. kris.balasub@gmail.com (K.B.); bengt.fadeel@ki.se (B.F.); kagan@pitt.edu (V.E.K.).

### SUPPLEMENTARY MATERIALS

[www.sciencesignaling.org/cgi/content/full/8/395/ra95/DC1](http://www.sciencesignaling.org/cgi/content/full/8/395/ra95/DC1)

Fig. S1. Comparison of PS- and TLCL-dependent phagocytosis by RAW 264.7 cells.

Fig. S2. CL-expressing liposomes are colocalized with lysosomes in RAW 264.7 cells and primary human macrophages.

Fig. S3. Integration of exogenous TLCL and the analysis of externalized CL on mitochondria.

Fig. S4. Gating strategy for the staining of mitochondria with FITC-conjugated annexin V.

Fig. S5. Phagocytosis of mitochondria presenting TLCL on their surface.

Fig. S6. Oxidation of TLCL-liposomes by soybean LOX.

Fig. S7. LC-MS analysis of the different molecular species of CL in *E. coli*.

Fig. S8. CL inhibits the nuclear translocation of NF- $\kappa$ B.

Fig. S9. Inhibition of the LPS-dependent production of cytokines is not a result of a loss in cell viability or the blocking of LPS by CL-liposomes.

Fig. S10. CL does not inhibit ATP-induced inflammasome activation in LPS-primed cells.

Fig. S11. The 2D structural representations of lipid A, TLCL, and *E. coli* CL.

Fig. S12. Comparison of the binding affinities of TLCL for MD2, TLR4, and TLR5.

Fig. S13. CL does not inhibit the flagellin-stimulated secretion of cytokines.

Fig. S14. Predicted binding poses of lipid A, TLCL, and lipid IVA to the TLR4-MD2 complex as determined by molecular docking simulations.

Table S1. The binding energies of lipid A, TLCL, and *E. coli* CLs with MD2.

**Author contributions:** K.B., V.E.K., and B.F. formulated the hypothesis; K.B. and V.E.K. designed the study and wrote the manuscript; K.B. performed phagocytosis, cytokine profiling, and binding experiments; A.M. and K.K. performed phagocytosis, cytokine profiling, and fluorescence microscopy experiments for HMDMs; B.F. designed the HMDM studies and contributed to the writing of the manuscript; J.S.L. contributed to the design of the MPM studies and the writing of the manuscript; J.S.L. and Z.X. performed experiments and analyzed data for the TGF- $\beta$  and gene expression studies; D.M. and J.K.-S. performed computational analysis; H.H.D. and J.F.J. established the mito-chondrial damage model and participated in the imaging experiments; C.M.S.C. and S.W. performed the imaging experiments and analyzed the data; Y.Y.T., V.A.T., V.I.K., and A.P. performed the LC-MS analysis of CLs, oxidized CLs, and mono-lyso-CLs; P.R. and R.K.M. contributed to data analysis and the writing of the manuscript; H.B. contributed to the development of the hypothesis, experimental design, data analysis, and the writing of the manuscript; and J.F.J. performed statistical analysis.

**Competing interests:** The authors declare that they have no competing interests.

<sup>4</sup>Center for Biologic Imaging, University of Pittsburgh, Pittsburgh, PA 15261, USA

<sup>5</sup>Division of Metabolic and Vascular Health, University of Warwick, Coventry CV4 7AL, UK

<sup>6</sup>Department of Internal Medicine, Acute Lung Injury Center of Excellence, University of Pittsburgh, Pittsburgh, PA 15213, USA

<sup>7</sup>Veterans Affairs Pittsburgh Healthcare System, Pittsburgh, PA 15215, USA

<sup>8</sup>Department of Critical Care Medicine, University of Pittsburgh School of Medicine, Pittsburgh, PA 15261, USA

## Abstract

Among the distinct molecular signatures present in the mitochondrion is the tetra-acylated anionic phospholipid cardiolipin, a lipid also present in primordial, single-cell bacterial ancestors of mitochondria and multiple bacterial species today. Cardiolipin is normally localized to the inner mitochondrial membrane; however, when cardiolipin becomes externalized to the surface of dysregulated mitochondria, it promotes inflammasome activation and stimulates the elimination of damaged or nonfunctional mitochondria by mitophagy. Given the immunogenicity of mitochondrial and bacterial membranes that are released during sterile and pathogen-induced trauma, we hypothesized that cardiolipins might function as “eat me” signals for professional phagocytes. In experiments with macrophage cell lines and primary macrophages, we found that membranes with mitochondrial or bacterial cardiolipins on their surface were engulfed through phagocytosis, which depended on the scavenger receptor CD36. Distinct from this process, the copresentation of cardiolipin with the Toll-like receptor 4 (TLR4) agonist lipopolysaccharide dampened TLR4-stimulated production of cytokines. These data suggest that externalized, extracellular cardiolipins play a dual role in host-host and host-pathogen interactions by promoting phagocytosis and attenuating inflammatory immune responses.

---

## INTRODUCTION

Since primordial times, prokaryotes and higher organisms have been waging a war for survival through adaptations enabled by evolutionarily imprinted plasticity in their genomes. Despite co-opting mutually advantageous endosymbiotic (1) and symbiotic (2) relationships, bacterial colonization is typically deleterious to the multicellular host. This has led to a “game” of pervasion and evasion, with the host deploying surveillance systems (3) to parse the tissue microenvironment for pathogen-associated molecular patterns (PAMPs) and pattern recognition receptors (PRRs) to target these pathogens for destruction (4). Timely and appropriate execution of these steps is crucial for reestablishment of tissue homeostasis (5, 6). In the turbulence of these interactions, it is crucial for the host defenses to distinguish self from nonself and to translate this difference into appropriate action—“hold fire” versus “destroy the intruder”—that is, tolerance versus annihilation, respectively. At the molecular level, the ability to make this distinction necessitates the existence of distinctive, pathogen-specific ligands that are not identifiable in host cells and vice versa. A number of such bacterial and host ligands, including cell wall polysaccharides, lipids, phospholipids, and their metabolites, have been identified as such critical signals (7, 8).

The aminophospholipid phosphatidylserine (PS) serves as a universal “eat me” signal that promotes the engulfment of apoptotic cells and membranes by macrophages (9). Whereas PS is found in most cellular and organellar membranes (10), it is absent from mitochondrial and bacterial membranes because of the activity of PS decarboxylase (11, 12). Instead, these membranes contain the signature phospholipid cardiolipin (CL), which plays critical structural and functional roles in bioenergetics (13). In addition to this role, mitochondrial CL was identified as a pro-survival, intracellular eat me signal that promotes the LC3-mediated removal of damaged mitochondria through the process of mitophagy (14). In contrast to such intracellular homeostatic controls, however, there are several reports indicating that cells release CL-presenting mitochondria and mitochondrial membranes under several pathophysiological scenarios, including neutrophil activation (15), stress, necrosis, and acute trauma (16, 17). Similarly, infections challenge the immune system by externalizing CL on the surface of bacterial membranes (18). Efficient clearance of these membranes is paramount, particularly because of the reported immunogenic effects of DNA and *N*-formyl peptides (19), thus raising the question of whether macrophages have the capabilities to identify and target extracellular, CL-presenting mitochondrial and bacterial membranes for degradation. Here, we report that CLs are effective extracellular eat me signals that promote phagocytosis whereby CL-dependent engulfment is mediated through the scavenger receptor (SR) CD36, which is found on the macrophage cell surface. When copresented with bacterial Toll-like receptor 4 (TLR4) agonist lipopolysaccharide (LPS), CL dampens TLR4-dependent cytokine production. These findings identify a dichotomous role for extracellular CL as an eat me signal to macrophages and as an inhibitor of the innate immune response.

## RESULTS

### CL-containing liposomes are recognized and engulfed by macrophages

To directly assess the contribution of CL to phagocytosis, we incubated macrophage cell lines, including RAW 264.7 cells and phorbol 12-myristate 13-acetate (PMA)-treated THP-1 cells, as well as primary human monocyte-derived macrophages (HMDMs) and mouse peritoneal macrophages (MPMs) with large unilamellar vesicles (LUVs; or liposomes) composed of tetralineoyl-cardiolipin (TLCL) in dioleoylphosphatidylcholine (DOPC). We observed a TLCL-dependent increase in the engulfment of these liposomes (Fig. 1, A to D), which was more substantial than the phagocytosis of liposomes containing other major phospholipids, including PS (fig. S1). Control experiments in the presence of cytochalasin D (CytD), an inhibitor of actin polymerization that is routinely used to verify phagocytosis, were consistent with the idea that engulfment of the liposomes occurred through a process of phagocytosis (Fig. 1, A to D). To assess what happened to the phagocytosed liposomes, we performed live cell-imaging experiments in which macrophages were labeled with lysosome-selective fluorescent dyes after phagocytosis. We observed marked (85%) compartmentalization of TLCL-liposomes to the lysosomes and their segregation from the cytoplasm (Fig. 1, E and F, and fig. S2), which suggested that the phagocytosed liposomes were delivered along the degradative, phagosomal, and lysosomal route.

## Mitochondria presenting CL on their surface are recognized and engulfed by macrophages

To establish the potential of mitochondria to be macrophage targets, we used two independent approaches to present CL at the mitochondrial surface. In the first model, the exogenous CL model, liver mitochondria were isolated through a two-stage, differential centrifugation protocol [P2 fractionation followed by density gradient centrifugation (20)] and then were incubated with TLCL, which was followed by an assessment of its integration efficiency and surface presentation, as well as of CL-dependent phagocytosis. We observed a ~50 to 60% integration efficiency for mitochondria incubated with exogenous TLCL (~13 to 19 nmol of TLCL/mg of protein) (fig. S3). Flow cytometric analysis of the binding of fluorescein isothiocyanate (FITC)-labeled annexin V to CL (14) verified that the lipid was indeed presented at the mitochondrial surface (Fig. 2A and fig. S4). Because annexin V also binds to other anionic phospholipids, including PS (a potential contaminant from copurified membranes), we used membrane-impermeable phospholipase A<sub>2</sub> (PLA<sub>2</sub>) to directly and quantitatively detect TLCL integrated on the mitochondrial surface (14). Liquid chromatography–mass spectrometry (LC-MS) analysis of mono-lyso-CL formed as a result of the action of PLA<sub>2</sub> on mitochondrial surface CL verified the surface presentation of TLCL (Fig. 2B). To assess phagocytosis, mitochondria labeled with MitoTracker Red were incubated with macrophages and then the phagocytosis of the mitochondria was assessed by flow cytometric analysis. Macrophages engulfed two- to fourfold more TLCL-presenting mitochondria than control mitochondria (Fig. 2C and fig. S5), which suggested that CL functioned as an extracellular eat me signal for the clearance of non-PS-presenting mitochondria by macrophages.

In the second model, the damaged mitochondria model, we used actinomycin D (ActD)-induced apoptosis of mouse embryonic fibroblasts (MEFs) to induce mitochondrial damage (21). To determine whether these mitochondria presented CL at their surface, we used annexin V–FITC to detect externalized CL on mitochondria that were isolated (in the P2 fraction) from these cells. Flow cytometric analysis revealed a threefold increase in the number of mitochondria stained with annexin V–FITC in ActD-treated MEFs compared to that in control, untreated MEFs (Fig. 2D). Direct assessment of CL at the surface of damaged mitochondria with PLA<sub>2</sub> in combination with LC-MS, as described earlier, revealed a twofold increase in the amount of CL cleaved from the surface of damaged mitochondria compared to that cleaved from the surface of control mitochondria (Fig. 2E and fig. S3D). Consistent with this observation, we observed about a threefold increase in the number of damaged mitochondria that were phagocytosed compared to the number of control mitochondria that were phagocytosed. This process was inhibited by annexin V because of its ability to bind to and shield CL, thereby preventing its interaction with macrophages (Fig. 2F).

## CL-dependent phagocytosis is impervious to acyl chain composition and peroxidation state

Because apoptotic cells that present peroxidized PS are more efficiently recognized by macrophages than are cells that present unoxidized PS (22), we investigated whether this was also true for CL-dependent phagocytosis. To this end, we used soybean lipoxygenase (LOX) (23) to selectively oxidize TLCL on the outer leaflet of preformed liposomes (fig.

S6). We found that there was no difference in the extent of phagocytosis of per-oxidized and unoxidized TLCL-liposome populations by RAW 264.7 cells (Fig. 3, A and B). Similarly, CL-liposomes with monounsaturated oleoyl-chains [tetraoleoyl-cardiolipin (TOCL)] were phagocytosed with about the same efficiency as were TLCL-liposomes (Fig. 3, A and B). Finally, we determined that CLs derived from *Escherichia coli* with a diverse combination of eight different acyl chains varying from a shorter C14:0 chain to longer C18:1 and C19:0 chains (fig. S7) were as effective as eukaryotic CLs in promoting phagocytosis (Fig. 3, C and D). Thus, the di-anionic polar heads of CLs, rather than their hydrophobic acyl chains, appear to act as determinants of the ability of CLs to stimulate phagocytosis.

### Phagocytosis of TLCL-liposomes depends on the macrophage SR CD36

Macrophages have evolutionarily adapted to identify and eliminate a multitude of danger signals through phagocytic degradation mechanisms realized through expression of several PRRs. Among these, members of the SR family participate in the recognition of PAMPs as well as of host-derived, damage-associated molecular patterns (DAMPs) (24). In experiments with a pan-SR inhibitor polyinosine (Poly I) (25), we observed a >70% reduction in the phagocytosis of TLCL-liposomes (Fig. 4A). Binding studies with recombinant proteins (Fig. 4B) and phagocytosis studies in the presence of blocking antibodies (Fig. 4C) (26, 27) identified the SR CD36 as the putative receptor that mediated the phagocytosis of TLCL-liposomes. To more definitively establish a role for CD36, we assessed phagocytosis by thioglycollate-elicited MPMs obtained from wild-type and *Cd36*-null mice (28). MPMs from the CD36-deficient mice demonstrated substantially reduced engulfment of TLCL-liposomes compared to that by macrophages from wild-type mice (Fig. 4, D to F), which suggests that CD36 mediates CL-dependent phagocytosis.

### CL dampens the inflammatory response to LPS

The primary initiator of the production of inflammatory cytokines after infection by Gram-negative bacteria is LPS, which is localized on the outer cell membrane of these pathogens. However, after infection, the bacterial outer membrane also becomes enriched in CL (18), which can potentially promote CD36-mediated clearance of bacterial membranes, thereby averting the LPS-dependent activation of TLR4. To understand how the copresentation of CL and LPS contributed to the ability of LPS to activate TLR4, we performed cytokine profiling analysis of RAW 264.7 cells (a mouse macrophage cell line) incubated with LPS alone or in the presence of CL-liposomes (Fig. 5). We observed a marked reduction in the LPS-induced secretion of the inflammatory cytokines interleukin-6 (IL-6), granulocyte-macrophage colony-stimulating factor (GM-CSF), IL-12, and the CXC chemokine CXCL10 (also known as IP-10) as a function of TLCL-liposome concentration (Fig. 5A). Analysis of cell lysates showed substantial TLCL-dependent reductions in the concentrations of intracellular pro-IL-1 $\alpha$  and pro-IL-1 $\beta$  (Fig. 5B) (29). Substituting TLCL-liposomes with *E. coli* CL-liposomes elicited similar results, whereas substitution with PC-liposomes or PS-liposomes had no effect on LPS-induced cytokine production, with the exception of CXCL10 (Fig. 5, B and C). Similar reductions in LPS-induced inflammatory cytokine secretion were observed in experiments with MPMs isolated from thioglycollate-treated mice (Fig. 5D).

We further showed the failure of LPS to induce the nuclear translocation of nuclear factor  $\kappa$ B (NF- $\kappa$ B) in macrophages when co-incubated with CL (fig. S8). These effects were not a result of the CL-liposomes inducing toxicity in the treated cells (fig. S9A). Furthermore, these effects could not be attributed to the binding and sequestration of negatively charged LPS to anionic TLCL-liposomes, as determined by enzyme-linked immunosorbent assay (ELISA)-based binding assays (fig. S9B). To determine whether TLCL inhibited LPS-induced responses in primary human macrophages, we performed cytokine expression analysis in M-CSF-differentiated macrophages obtained from affinity-purified, CD14<sup>+</sup> peripheral blood mononuclear cells (PBMCs). The ability of LPS to stimulate the secretion of inflammatory cytokines was substantially compromised by the copresentation of TLCL-liposomes (Fig. 5E). Similar to their effect on LPS-induced proinflammatory cytokine secretion, TLCL-liposomes also inhibited the LPS-dependent production of the anti-inflammatory cytokine transforming growth factor- $\beta$  (TGF- $\beta$ ) (Fig. 6A) (30, 31). Furthermore, quantitative polymerase chain reaction (qPCR) analysis revealed that TLCL-liposomes inhibited the LPS-induced expression of *inducible nitric oxide synthase 2* (*NOS2*) and *arginase-1* (*ARG1*) in MPMs (Fig. 6, B and C). These results are consistent with the reported control of *NOS2* expression downstream of TLR4 activation and of the regulation of *ARG1* expression through IL-6-dependent autocrine responses (30, 32). Thus, the ability of TLCL-liposomes to inhibit both pro- and anti-inflammatory responses is supported by their inhibition of the genes encoding the macrophage markers *NOS2* and *ARG1*, which are representative of the M1 (classically activated) and M2 (alternatively activated) macrophage phenotypes, respectively, or variants thereof (33, 34).

### **The CD36-dependent internalization of CL is not required for its inhibition of LPS-induced responses**

Because several reports have emphasized cooperative interactions between CD36 and TLRs, with cross-activating roles in inflammation and phagocytosis (35), we investigated whether the engulfment of TLCL-liposomes through CD36 or potential interactions between CD36 and TLR4 might be critical for the attenuation of LPS signaling by CL. We analyzed the production of cytokines by thioglycollate-elicited MPMs from *Cd36* knockout animals. We found that TLCL-liposomes inhibited the LPS-induced production of cytokines by *Cd36*-deficient cells (Fig. 6, D and E), which suggests that CD36 and the CD36-mediated internalization of CL are not required for the inhibition of LPS-induced cytokine production.

### **The impairment of LPS-induced responses by CL occurs at the cell surface**

Because the copresentation of LPS and CL inhibited TLR4 signaling through pathways mediated either by MyD88 (myeloid differentiation primary response 88), in the case of IL-6, GM-CSF, and pro-IL-1, or by TRIF (Toll/IL-1 receptor domain-containing adaptor-inducing interferon- $\beta$ ), in the case of CXCL10 (Fig. 5) (36), it seemed likely that the target of CL was upstream of both of these adaptor proteins. Furthermore, because the inhibition of TLR4-dependent signaling did not require the internalization of TLCL-liposomes through CD36 (Fig. 6, D and E), we hypothesized that extracellular rather than intra-cellular mechanisms were operative in eliciting this inhibition. To test this possibility, we either pre-incubated (primed) macrophages with LPS before the addition of TLCL-liposomes or co-incubated the macrophages with both LPS and TLCL-liposomes. We found that the TLCL-

liposomes inhibited cytokine secretion by macrophages when co-incubated with LPS but not when added to LPS-primed macrophages (Fig. 6F). In addition, our earlier observations that TLCL was predominantly sequestered into lysosomes and segregated from the cytoplasm (Fig. 1, E and F, and fig. S2) raised the possibility that cytoplasmic, inflammasome-dependent pro-IL-1 activation pathways would be unaffected by CL. This was indeed supported by our observations that TLCL-liposomes failed to inhibit the adenosine triphosphate (ATP)-induced secretion of activated IL-1 $\alpha$  and IL-1 $\beta$  (37) by LPS-primed macrophages (fig. S10). These observations are suggestive of an extracellular, rather than intracellular, control of cytokine responses by extracellular CLs, which may act by preventing LPS from effectively engaging and activating TLR4 at the macrophage surface.

### **Inhibition of inflammatory cytokine secretion by CL occurs by blocking MD2**

The activation of TLR4 is incumbent upon the ability of LPS-bound myeloid differentiation protein 2 (MD2) to engage TLR4 monomers and trigger the assembly of functionally active (TLR4/MD2)<sub>2</sub> heterotetrameric complexes (38, 39). Because of this critical requirement of LPS-bound MD2 for TLR4 activation and because of the general structural similarity between TLCL and *E. coli* CL and lipid A, the biologically active component of LPS (Fig. 7A and fig. S11), we reasoned that CL might interfere with LPS-MD2 interactions. Indeed, competitive binding experiments demonstrated the ability of TLCL-liposomes, but not PC- or PS-liposomes, to inhibit the binding of LPS to MD2 (Fig. 7B). To gain further structural insights into the potential interactions between CL and MD2, we performed molecular docking studies. We determined that lipid A, TLCL, and *E. coli* CLs (17:1/15:0/16:0/18:1-CL and 17:1/17:1/15:0/16:0-CL) showed similarities in their binding poses with MD2 (Fig. 7C) and similarities in binding energies for the top-ranked models (table S1). We also noted substantial overlaps in the amino acid residues of MD2 that interacted with lipid A and the CLs (Fig. 7D). In contrast, substituting MD2 with TLR4 alone (no MD2) or with an unrelated TLR, such as TLR5 [which is activated by flagellin (40)], in our docking experiments yielded markedly lower binding affinities (fig. S12). Furthermore, unlike MD2 (Fig. 7C), neither TLR4 nor TLR5 had a consensus CL-binding motif. Consistent with these data, TLCL did not inhibit TLR5-dependent cytokine secretion in RAW 264.7 cells (fig. S13).

Thus, these data support a mechanism in which CL does not directly engage TLRs but rather interacts with MD2, a TLR4-associated protein. This model was illustrated by substituting MD2 with the biologically relevant heterotetramer (TLR4/MD2)<sub>2</sub> in our docking studies, which demonstrated the preferential binding of lipid A and TLCL to MD2 in this complex, yielding similar binding poses and energies (fig. S14). Finally, in contrast to lipid A (fig. S14D, magnified view), both CL and the TLR4 antagonist lipid IVA (41) showed limited engagement with the opposing TLR4 (TLR4\*) in the (TLR4/MD2)<sub>2</sub> complex (fig. S14, E and F, magnified views). On the basis of these data, and the reported critical need for bridging interactions between LPS-MD2, TLR4, and TLR4\* for receptor activation (38, 41), we suggest that the inhibition of TLR4 activation by CL stems from its ability to bind to MD2, but its inability to engage TLR4\* and promote oligomerization.

## DISCUSSION

Phagocytosis and immune surveillance are two distinct, yet interrelated, functions that complement each other in maintaining tissue homeostasis (3). The identification, capture, and elimination of pathogens and cells with atypical signatures (42) through phagocytosis is achieved through the expression of ligand-selective receptors (for example, Tim-4 for PS and CD206 for man-nose) or multiple PRRs (for example, CD204, SRB I/II, CD36, and CXCL16), which are further diversified and enhanced by bridging proteins [including thrombospondin-1 (TSP-1), milk fat globule-EGF factor 8 (MFG-E8), growth arrest-specific 6 (Gas-6), and  $\beta$ -2-glycoprotein I] and their receptor partners (for example, Mer, the integrin  $\alpha_5\beta_3$ , CD36, and lipoprotein receptor-related protein) (43,44). Because of the established roles for PS (5,6) and CL(14) as extracellular and intracellular clearance signals, respectively, and because of reports on the externalization of CLs during host-pathogen encounters (18, 19), we hypothesized that CL might fulfill yet another role as an extracellular eat me signal. Indeed, we demonstrated that CL functioned as a CD36-dependent prophagocytic eat me signal with efficacies exceeding those of PS. Despite general similarities between PS and CL in terms of their role as recognition signals, the specific mechanisms by which they lead to engulfment by macrophages seem to be markedly different. Indeed, host and bacterial CLs, which have largely different lengths and levels of unsaturation of their acyl chains, were equally effective as eat me signals. Furthermore, in contrast to the effect of acyl chain peroxidation on PS-dependent phagocytosis (22, 45), oxidation of the acyl chains of CL did not affect phagocytic efficiency.

The mannose receptors CD206 and MRC1/2 and the SRs make substantial contributions to nonsterile and sterile pathology by facilitating the clearance of PAMPs and DAMPs. Whereas CD206 mediates the endocytic clearance of bacteria and glycoproteins that present mannose (46, 47), SR-A (CD204) accepts a broader range of ligand patterns, including bacterial surface components and host-derived DAMPs, such as oxidized lipids and lipoproteins (24). In addition, SR-B family members, including CD36, mediate the recognition of intra-cellular bacterial and eukaryotic proteins (26). This supports the notion that neutrophil-induced damage to the bacterial cell wall during infection (48) can indeed provide macrophages with access to cytoplasmic constituents and to CL associated with the bacterial membrane. Similarly, trauma is likely to lead to macrophages encountering CL-containing mitochondrial fragments (19). On the basis of our binding experiments and phagocytosis studies, we conclude that macrophage CD36, rather than SR-A, contributes to the clearance of such CL-containing membranes. Notwithstanding the indirect roles of bacterial and mitochondrial chemotactic peptides and nucleic acids to phagocytosis (19, 49), our results suggest that host- and pathogen-derived CLs make direct contributions to the elimination of these non-PS-containing entities by macrophages. We would expect that this role for CL as a signal for the clearance of mitochondrial and bacterial membranes predominates over a potential role for CL at the cell surface (50), which is dominated by PS, a well-established phagocytic signal (5, 9).

In parallel with phagocytosis, immune surveillance systems, including the TLRs and inflammasomes, have evolved with the goals of containing localized disturbances in

inflammatory homeostasis and maintaining tissue defense mechanisms should the engulfment machinery be compromised or overwhelmed, as is the case during infection. Despite these collaborative fail-safe mechanisms, higher-order organisms are challenged by multiple evasion strategies adopted by pathogens for their survival and dissemination (51–53). Given the ability of CLs to stimulate CD36-dependent phagocytosis by macrophages, as well as the structural similarities between this phospholipid and the LPS component lipid A, we examined the possibility that CLs might modulate TLR4 activation. We found that the CL-dependent inhibition of LPS-induced TLR4 activation was independent of CD36 (54) and was mediated by an extracellular mechanism independent of CL internalization. Indeed, similar relationships between eat me signals, phagocytosis, and the modulation of cytokine signaling have been reported in macrophages challenged with apoptotic cells presenting PS at their surface (55).

Although lipid-binding proteins such as CD14 and LPS-binding protein (LBP) (56, 57) facilitate the transfer of LPS to MD2, loss of these proteins is not detrimental to LPS-MD2 binding (58–60). Moreover, unlike the limited selectivity of CD14 and LBP for lipid species (61), CL selectively competed with LPS for binding to MD2, unlike PC and PS. Accordingly, the CL-dependent repression of both pro- and anti-inflammatory cytokine responses, including the reduced expression of *NOS2* and *ARG1*, is dependent on cell surface TLR4 (30, 32). In contrast, inhibition of cytokine secretion by macrophages challenged with PS on the surface of apoptotic cells occurs through intracellular mechanisms such as the TGF- $\beta$ -dependent ubiquitylation of MyD88 (62) or through TGF- $\beta$ -independent mechanisms that are mediated by the zinc finger nuclear factor, GC-binding protein (55), peroxisome proliferator-activated receptor- $\delta$  (PPAR $\delta$ ) (63), or nuclear receptor liver X receptor (LXR) (64).

Many studies have implied a role for PAMPs in the etiology of chronic inflammation and autoimmune disease (65, 66), an association that is believed to stem from molecular mimicry between pathogen-derived antigenic determinants and evolutionarily conserved motifs in eukaryotes. In this context, it is notable that CL, an ancient prokaryotic phospholipid, has been retained by the mitochondria, an organelle that is considered to have evolved from eubacterial ancestors (67). Our observations on the dual functions of CL as a phagocytic ligand and a modulator of TLR4 signaling have implications for host defense and the restoration of homeostasis. On the basis of our findings, the copresentation of bacterial CL with LPS (18) might represent an alternative evasion strategy, similar to the use of underacylated LPS (68) by certain Gram-negative bacteria (69), to subdue immune surveillance mediated by TLR4. However, this adaptation would also likely render these pathogens vulnerable to clearance through CD36-dependent phagocytosis. Thus, evolutionary conservation of CD36 is a beneficial adaptation for the host; a counter-response to the use of CLs by Gram-negative bacteria to incapacitate innate immune signaling. Host and bacterial CLs may also be of additional benefit to the host during the reparative phase of tissue injury in which infiltrating macrophages engulf host- and pathogen-derived damaged membranes and cells in tandem with the resolution of inflammation and restoration of homeostasis. These considerations are consistent with observations that the abundance of CD36 is transcriptionally regulated by Nrf2 and PPAR $\gamma$

in activated and inflammatory macrophages (70) and that an increase in CD36 abundance resolves inflammation through PPAR $\gamma$ -dependent pathways (71). Similar roles have also been established for the mannose receptor, which is present in low abundance during inflammation but becomes more abundant during the resolution phase of inflammation (46, 72).

In conclusion, our data suggest that extracellular CLs may be used by both eukaryotes and prokaryotes for their own benefits, through CD36-dependent clearance and suppression of TLR4-dependent immune responses, respectively. Although many inhibitors of TLR signaling are known (73), we present an example of the extracellular control of TLR4 function by a molecular pattern shared by both a host and a pathogen. Overall, our results suggest that extracellular CLs represent a phospholipid species that share attributes of PAMPs and DAMPs, and imply that trapping or targeting CLs may have broad repercussions for inflammation, sepsis, tissue repair, and autoimmunity.

## MATERIALS AND METHODS

### Materials

Cell culture media, heat-inactivated fetal bovine serum (FBS), Hanks' balanced salt solution, Lipofectamine, DiI, MitoTracker Red CMXRos (MitoTracker Red), LysoTracker Deep Red, ER-Tracker Blue-White, and fluorescently labeled secondary antibodies were from Life Technologies, and FITC-conjugated annexin V was from Trevigen Inc. DOPC, dioleoylphosphatidylserine (DOPS), dioleoylphosphatidylethanolamine (DOPE), TLCL, TOCL, *E. coli* CL, and the fluorescent phospholipids NBD-CL, NBD-PC, and N-NBD-PE were obtained from Avanti Polar Lipids. Blocking antibodies specific for CD36 (ab23680) and SRB I/II (ab36970) and isotype controls were obtained from Abcam, antibodies against p65 were from Santa Cruz Biotechnology, and anti-human CD14 microbeads were from Miltenyi Biotec. Biotinylated LPS was obtained from InvivoGen. Recombinant MD2 was a gift from J. Weiss (Departments of Internal Medicine and Microbiology, University of Iowa, Coralville, IA). His-tagged recombinant proteins corresponding to the extracellular domains of CD36 and CD204 were purchased from R&D Systems. Recombinant M-CSF protein was obtained from Novakemi. AlamarBlue and LDH viability and toxicity kits were from Promega. Organic solvents, soy bean LOX, DAPI, CytD, ATP, PLA<sub>2</sub> from porcine pancreas, Poly I, LPS from *E. coli* 055: B5, ovalbumin, bovine serum albumin (BSA), and all other biochemical reagents were purchased from Sigma-Aldrich. Normal and reversed-phase chromatography columns (150  $\times$  1 mm) were from Phenomenex.

### Primary cells and cell lines

RAW 264.7 and THP-1 cells were obtained from the American Type Culture Collection and were cultured in Dulbecco's modified Eagle medium (DMEM; for RAW 264.7 cells) or RPMI 1640 (THP-1), each containing 10% FBS. THP-1 cells were differentiated into macrophages by being cultured in the presence of PMA (40 pmol/10<sup>6</sup> cells) for 72 hours before experiments were performed. PBMCs were prepared from buffy coats obtained from healthy blood donors by density gradient centrifugation as previously described (74) and then were positively selected with CD14 microbeads. Blood was obtained in accordance

with Institutional Review Board guidelines at Karolinska University Hospital, Stockholm, Sweden. To obtain HMDMs, CD14-positive monocytes were cultured for 3 days in RPMI 1640, 10% FBS containing M-CSF (50 ng/ml). C57BL/6J and *Cd36*<sup>-/-</sup> (B6.129S1-Cd36tm1Mfe/J) mice were obtained from the Jackson Laboratory. The *Cd36*<sup>-/-</sup> mice were backcrossed to C57BL/6J mice for 11 generations and then subsequently crossed to *Cd36*<sup>-/-</sup> mice from the Blood Research Institute (gift of R. Silverstein, Blood Center of Wisconsin Inc., Milwaukee, WI) before establishing the colony here at the University of Pittsburgh. All experimental procedures were performed in age-matched (6- to 8-week-old) and gender-matched mice. The animals were housed and maintained in a pathogen-free environment, and studies were conducted in accordance with the Institutional Animal Care and Use Committee at the University of Pittsburgh. MPMs were isolated from wild-type (C57BL/6) and *Cd36*<sup>-/-</sup> mice as previously described (28). Briefly, macrophages were harvested from the peritoneal cavity of the mice 96 hours after they received an intraperitoneal injection of 3% (w/v) thioglycollate. Cells were manually counted with a hemocytometer. Cytospins confirmed that ~90 to 95% of the harvested cells were macrophages. MEFs were cultured in DMEM-high glucose (DMEM-HG) containing 15% FBS and supplemented as described previously (75).

## Liposomes

Liposomes composed of DOPC (PC-liposomes), DOPS/DOPC (0.3:0.7 mol/mol) (PS-liposomes), DOPE/DOPC (0.3:0.7 mol/mol) (PE-liposomes), or TLCL/DOPC (0.3:0.7 mol/mol) (TLCL-liposomes) were used for most experiments. In some experiments, TLCL was substituted with CLs containing symmetric or asymmetric acyl chain molecular species, which are indicated in the appropriate text and figure legends. In addition to the lipids listed earlier, fluorescent liposomes used in the phagocytosis experiments contained N-NDB-PE or DiI at a final concentration of 0.5 mol % (44) to monitor phagocytosis by flow cytometry or microscopy, respectively. Fluorescent liposomes prepared for the colocalization experiments contained NBD-CL or NBD-PC at 1 mol % in PC. Liposomes were prepared through an extrusion procedure. Briefly, lipids were dried down with a stream of nitrogen gas, which was followed by the application of a high vacuum to remove trace organic solvents. The dried film was then hydrated in tris-buffered saline [TBS; 20 mM tris (pH 7.2), 150 mM NaCl] and vortexed for ~1 min to give a multilamellar dispersion, which was extruded 11 times through polycarbonate membranes (100-nm pore size) to give LUVs. Peroxidized LUVs were prepared by incubating LUVs with soybean LOX (2000 U/mg of lipid) for 16 hours at 37°C on an Eppendorf ThermoMixer set at a speed of 900 rpm. Oxidation was verified by absorption spectroscopy ( $A_{235}$ ) followed by LC-MS analysis.

## Isolation of mitochondria

Mitochondria were isolated from mouse livers by Percoll gradient differential centrifugation as described previously (20). All homogenization procedures were performed on ice, and centrifugations were performed at 4°C. Perfused livers from C57BL/6 mice were minced into small pieces in mitochondria isolation buffer [MIB; 210 mM mannitol, 70 mM sucrose, 10 mM Hepes, 1 mM EDTA (pH 7.4)] containing protease inhibitors and then were homogenized with a motorized homogenizer (1600 rpm, 10 strokes). The homogenate was clarified by centrifugation at 700g for 10 min, and the supernatant was centrifuged at 7000g

for 10 min to pellet the crude mitochondrial fraction (P2). The P2 pellet was resuspended in 15% Percoll in MIB and layered over a 23 to 40% step gradient. After centrifugation at 30,000g for 7 min, the pure mitochondrial fraction (found at the interface between the layers of 23 and 40% Percoll) was washed and resuspended in MIB at a final concentration of 5 mg/ml. Alternatively, mitochondria were isolated from MEFs. MEFs ( $\sim 5 \times 10^6$  cells) in serum-free DMEM-HG were first incubated for 30 min in a CO<sub>2</sub> incubator with 1.5  $\mu$ M MitoTracker Red. The cells were then washed with phosphate-buffered saline (PBS) to remove excess MitoTracker Red and layered with DMEM-HG containing 10% FBS. This was followed by the addition of ActD (100 ng/ml) and incubation for 20 hours in a CO<sub>2</sub> incubator to induce apoptosis. After 20 hours, untreated and ActD-treated MEFs were trypsinized and centrifuged, and the cell pellets were homogenized and centrifuged to obtain the P2 mitochondrial fraction as described earlier, which was then used for further experiments.

### Integration of exogenous CL into mitochondria

Isolated mitochondria labeled with 1  $\mu$ M MitoTracker Red were incubated with TLCL at various ratios (0 to 80 nmol of TLCL/mg of mitochondrial protein) for 40 min at 22°C. The mitochondria were then washed, centrifuged at 15,000g for 4 min, and resuspended in TBS at a final concentration of 1 mg/ml before being subjected to lipid extraction and LC-MS analysis or being used for phagocytosis experiments.

### Assessment of externalized CL

Mitochondria were analyzed for the presence of externalized CL by flow cytometry as described previously (14). Briefly, 10  $\mu$ g of uncoated (control) and TLCL-coated liver mitochondria was resuspended in 500  $\mu$ l of TBS (pH 7.4) containing annexin V-FITC in the absence (negative control) or presence of 200  $\mu$ M Ca<sup>2+</sup>. The samples were analyzed on a Becton-Dickinson FACSCanto flow cytometer, and the data are presented as the percentage of the mitochondria that were annexin V-positive. A similar protocol was used for mitochondria isolated from MEFs with the exception that TBS was replaced with MIB. Quantitative analysis of CL content on the mitochondrial surface was performed as described previously (14). Briefly, control, TLCL-integrated, and damaged mitochondria were treated with PLA<sub>2</sub> (from porcine pancreas, 0.7 U/mg of protein) for 50 min at 4°C in the presence of fatty acid-free human serum albumin [2% (w/v)] to bind the hydrolysis products and prevent membrane damage. Lipids were extracted and then analyzed by LC-MS to determine the amounts of CL and mono-lyso-CL.

### Lipidomics analysis

Lipids were extracted using the Folch procedure (76). LC-MS was performed with a Dionex UltiMate 3000 high-performance liquid chromatography (HPLC) coupled on-line to a Q Exactive hybrid quadrupole-orbitrap mass spectrometer (Thermo Fisher Scientific). LC/electrospray ionization (ESI)-MS analysis was performed on a Dionex HPLC system (using the Chromeleon software), consisting of a Dionex UltiMate 3000 mobile phase pump, equipped with an UltiMate 3000 degassing unit and UltiMate 3000 autosampler (sampler chamber temperature was set at 4°C). The Dionex HPLC system was coupled to an LXQ ion

trap MS or to a hybrid quadrupole-orbitrap mass spectrometer. To analyze CL peroxidation, CL was separated by two-dimensional (2D) high-performance thin-layer chromatography and analyzed by LC-MS. Lipids were separated on normal phase [Luna 3  $\mu\text{m}$  Silica (2) 100  $\text{\AA}$ ] or reversed-phase (C18) columns (Phenomenex) at 30°C with a flow rate of 0.2 ml/min, which was followed by LC-MS analysis with a Finnigan LXQ linear ion trap mass spectrometer equipped with the Xcalibur operating system (Thermo Electron). The ESI probe was operated at a voltage of 5.0 kV in the negative ion mode, maintaining the capillary temperature at 150°C. MS<sup>n</sup> analysis of CL species was carried out as described earlier (22) to determine the fatty acid composition.

### Phagocytosis assays

Macrophages were washed with PBS (pH 7.4), layered with 300  $\mu\text{l}$  of serum-free medium, and incubated for 60 min in a CO<sub>2</sub> incubator with fluorescent LUVs (0 to 38 nmol of total lipid and 0 to 12 nmol of CL) or MitoTracker Red-labeled mitochondria (30 to 100  $\mu\text{g}$  of protein). Macrophages were washed to remove unbound targets (LUVs or mitochondria) and trypsinized briefly to remove surface-bound targets before being assessed for their phagocytosis by flow cytometry. For CytD and anti-CD36 antibody inhibition experiments, macrophages were preincubated for 20 min with 20  $\mu\text{M}$  CytD or antibodies (concentrations as indicated in the figure legends) before the addition of the LUVs. For Poly I inhibition experiments, the inhibitor and LUVs were successively added to the macrophages. To test the effects of annexin V on phagocytosis, 30  $\mu\text{g}$  of mitochondria was preincubated at 4°C for 15 min with 20  $\mu\text{g}$  of annexin V in the presence of 50  $\mu\text{M}$  Ca<sup>2+</sup> before being transferred to macrophages in serum-free medium. The final concentration of annexin V during the phagocytosis assay was 20  $\mu\text{g}/\text{ml}$ .

### Cytokine and qPCR analyses

To determine the amounts of proinflammatory cytokines produced, macrophages ( $\sim 0.5 \times 10^6$  cells) were incubated for 4 hours in serum-free medium (DMEM or RPMI 1640) containing 0.5% BSA, which was followed by the sequential addition of LPS (100 ng/ml) and then LUVs (0 to 38 nmol/ml). Cell culture medium (which was centrifuged to remove cells and debris) was recovered, and whole-cell lysates were prepared 16 hours later and submitted to the Luminex Core Facility at the University of Pittsburgh Cancer Institute (UPCI) for analysis or were analyzed at the Luminex facilities at Karolinska Institute as described previously (77). For LPS priming experiments, macrophages were incubated with LPS alone for 4 or 8 hours, followed by the addition of LUVs and further incubation for 4 hours before the cell culture media were recovered. To analyze TGF- $\beta$  production as well as *ARG1* and *NOS2* expression, MPMs from C57BL/6J mice (eight male mice) were plated on six-well plates at  $2 \times 10^6$  cells per well to obtain eight independently matched data sets for each of the treatments. Macrophages in RPMI 1640 containing 0.5% BSA were incubated for 60 min at 37°C in a CO<sub>2</sub> incubator with LPS (10 ng/ml) in the absence or presence of PC-liposomes or TLCL-liposomes (22.4 nmol of TLCL/ml). After 60 min, the medium was supplemented with FBS [10% (v/v) final], and the cells were incubated for a further 16 hours. The cell culture medium was harvested for the assessment of TGF- $\beta$  abundance by ELISA, whereas the cells were solubilized in QIAzol reagent. Total RNA was purified with the miRNeasy Mini Kit (Qiagen). Briefly, after phase separation with chloroform, the

aqueous phase containing the RNA was mixed with 1.5 volumes of 100% ethanol and loaded onto an RNeasy Mini spin column. After several washes with wash buffer, total RNA was resuspended in nuclease-free water. The quality of the RNA was examined by electrophoresis to exclude RNA degradation, and the concentration and purity of the RNA were measured with a NanoDrop spectrophotometer. RNA samples were reverse-transcribed to generate complementary DNA (cDNA) with SuperScript III Reverse Transcriptase (Moloney murine leukemia virus reverse transcriptase, Invitrogen). Quantitative real-time PCR (qPCR) analysis was performed according to the manufacturer's protocol (Applied Biosystems) by incubating the cDNA samples with the appropriate probes and primers of interest and TaqMan Universal PCR Master Mix II, and PCR amplification was measured with the 7900HT Real-Time PCR System. Probes and primers specific for *NOS2* (Mm00440502\_m1), *ARG1* (Mm01190441\_g1), and *18S* ribosomal RNA were obtained commercially (Applied Biosystems). Gene expression was analyzed by the  $C_t$  (cycle threshold) method, with *18S* rRNA serving as the endogenous control. The average  $C_t$  value of unstimulated wild-type control cells was used for normalization.

### Detection of NF- $\kappa$ B

Serum-starved macrophages cultured in DMEM or RPMI containing 0.5% BSA in glass-bottomed petri dishes were incubated for 60 min at 37°C with LPS in the absence or presence of PC-liposomes or TLCL-liposomes (11.4 nmol of TLCL). The macrophages were washed with PBS (pH 7.4) and fixed with 2% paraformaldehyde (PFA). To detect NF- $\kappa$ B, the macrophages were permeabilized with 0.2% Triton X-100 for 10 min, blocked with 2% BSA for 10 min, and then incubated for 60 min with anti-NF- $\kappa$ B antibody (sc-109, 2  $\mu$ g/ml). The dishes were then washed and incubated with DAPI (2  $\mu$ g/ml) and Alexa Fluor 488-conjugated anti-rabbit immunoglobulin G (5  $\mu$ g/ml). The dishes were finally washed, fixed with 2% PFA, and stored in PBS overnight at 4°C before being imaged.

### Fluorescence imaging analysis

For colocalization studies, macrophages incubated with NBD-CL-labeled liposomes were loaded with a combination of LysoTracker Deep Red and ER-Tracker Blue-White. Images were obtained with a Nikon TI inverted microscope equipped with a swept field confocal head. 3D stacks were collected with a 1.49-numerical aperture oil objective lens. Images were deconvolved with the 3D Landweber deconvolution capabilities of Nikon NIS-Elements software. Deconvolved images were imported into Imaris software (Bitplane Company), the lysosomal and NBD signals were segmented, and the degree of colocalization was calculated with the spots function. Colocalization studies with HMDMs used a Zeiss LSM 510 Meta confocal microscope, and data were analyzed with LSM Meta software. For all other fluorescence imaging experiments, we used a Nikon Eclipse TI confocal microscope equipped with an NIS-Elements acquisition and analysis software package. Projection images were generated off-line from acquired z-stack data.

### Lipid dot blot analysis

Serial dilutions (beginning at 5.7 nmol/50  $\mu$ l of TBS) of PC and CL were immobilized on PVDF membranes. The membranes were blocked with 1% ovalbumin for 60 min, which

was followed by incubation for 2 hours with 5.8 nM His-tagged recombinant proteins corresponding to the extracellular domains of CD204 and CD36 in TBS containing 1% ovalbumin and supplemented with 150  $\mu\text{M}$   $\text{Ca}^{2+}$ . The membranes were incubated with HRP-conjugated anti-His tag antibody, washed thrice with TBS, and then visualized with an enhanced chemiluminescent imaging system.

### Competitive binding analysis

Recombinant MD2 protein (50 ng) was immobilized overnight at 4°C on 96-well ELISA plates. The plates were blocked with 0.5% ovalbumin for 60 min and then incubated for 90 min with 509 ng of biotinylated LPS in the absence or presence of PC-liposomes, PS-liposomes, or TLCL-liposomes. The plates were washed, incubated for 60 min with HRP-conjugated streptavidin, and visualized by TMB-ELISA (450 nm).

### Molecular docking simulations

Avogadro software (version 1.1.1, 2013) (78) was used to generate the 3D structures of lipids, including lipid A and TLCL, with data obtained from the LIPID MAPS Lipidomics Gateway. The lipids were docked onto the crystal structure of MD2 extracted from the (TLR4-MD2)<sub>2</sub> het-erodimer (Protein Data Bank ID, 3VQ2) (79) with the AutoDock Vina program (<http://vina.scripps.edu>) (80). Lipid and protein structures were converted from pdb to pdbqt format with MGLTools (81). A grid box was centered at the -7.906, 29.837, and -2.185 coordinates with 60, 60, and 50 Å units in the *x*, *y*, and *z* directions, respectively, to cover the entire protein. AutoDock Vina reports the nine lowest energy conformations, which were inspected with PyMOL software ([www.pymol.org](http://www.pymol.org)). From the lowest energy conformation model, interacting amino acids of MD2 that are within a proximity radius of 5 Å to the lipids were identified.

### Statistical analysis

Results are presented as means  $\pm$  SD from at least three experiments. Data were analyzed with the Student's *t* test or by one-way analysis of variance (ANOVA) with Turkey's post hoc analysis. Data from experiments comparing TGF- $\beta$  production and *ARG1* expression among groups were tested with a nonparametric Friedman's test because the assumption of normality was not verified and the sample sizes were relatively small. In the presence of a statistically significant overall test, follow-up pairwise comparison was performed, and the *P* values were adjusted by the Bonferroni correction. For all the tests, *P* < 0.05 was considered to be statistically significant.

### Supplementary Material

Refer to Web version on PubMed Central for supplementary material.

### Acknowledgments

We thank J. Weiss (Departments of Internal Medicine and Microbiology, University of Iowa, Coralville, IA) for his gift of recombinant MD2 and R. Silverstein (Blood Center of Wisconsin Inc., Milwaukee, WI) for providing us with Cd36<sup>-/-</sup> mice to establish our colony.

**Funding:** This study was supported by grants from the NIH (PO1 HL114453, HL086884, U19AI068021, ES020693; NS076511, NS061817, CA165065; NIOSH OH008282), the Human Frontier Science Program (HFSP-RGP0013/2014), the Swedish Research Council, and a Core grant to the UPCI Cancer Biomarkers Facility/Luminex Core Laboratory (P30CA047904).

## REFERENCES

1. Diekmann Y, Pereira-Leal JB. Evolution of intracellular compartmentalization. *Biochem. J.* 2013; 449:319–331. [PubMed: 23240612]
2. Brestoff JR, Artis D. Commensal bacteria at the interface of host metabolism and the immune system. *Nat. Immunol.* 2013; 14:676–684. [PubMed: 23778795]
3. Senovilla L, Galluzzi L, Zitvogel L, Kroemer G. Immunosurveillance as a regulator of tissue homeostasis. *Trends Immunol.* 2013; 34:471–481. [PubMed: 23891238]
4. Thaiss CA, Levy M, Suez J, Elinav E. The interplay between the innate immune system and the microbiota. *Curr. Opin. Immunol.* 2014; 26:41–48. [PubMed: 24556399]
5. Michlewska S, McColl A, Rossi AG, Megson IL, Dransfield I. Clearance of dying cells and autoimmunity. *Autoimmunity.* 2007; 40:267–273. [PubMed: 17516208]
6. Tanaka M, Miyake Y. Apoptotic cell clearance and autoimmune disorder. *Curr. Med. Chem.* 2007; 14:2892–2897. [PubMed: 18045134]
7. Fullerton JN, O'Brien AJ, Gilroy DW. Lipid mediators in immune dysfunction after severe inflammation. *Trends Immunol.* 2014; 35:12–21. [PubMed: 24268519]
8. Denk S, Perl M, Huber-Lang M. Damage- and pathogen-associated molecular patterns and alarmins: Keys to sepsis. *Eur. Surg. Res.* 2012; 48:171–179. [PubMed: 22653136]
9. Fadeel B, Xue D. The ins and outs of phospholipid asymmetry in the plasma membrane: Roles in health and disease. *Crit. Rev. Biochem. Mol. Biol.* 2009; 44:264–277. [PubMed: 19780638]
10. Leventis PA, Grinstein S. The distribution and function of phosphatidylserine in cellular membranes. *Annu. Rev. Biophys.* 2010; 39:407–427. [PubMed: 20192774]
11. Voelker DR. Phosphatidylserine decarboxylase. *Biochim. Biophys. Acta.* 1997; 1348:236–244. [PubMed: 9370338]
12. Vance JE, Tasseva G. Formation and function of phosphatidylserine and phosphatidylethanolamine in mammalian cells. *Biochim. Biophys. Acta.* 2013; 1831:543–554. [PubMed: 22960354]
13. Milevskaya E, Dowhan W. Cardiolipin membrane domains in prokaryotes and eukaryotes. *Biochim. Biophys. Acta.* 2009; 1788:2084–2091. [PubMed: 19371718]
14. Chu CT, Ji J, Dagda RK, Jiang JF, Tyurina YY, Kapralov AA, Tyurin VA, Yanamala N, Shrivastava IH, Mohammadyani D, Qiang Wang KZ, Zhu J, Klein-Seetharaman J, Balasubramanian K, Amoscato AA, Borisenko G, Huang Z, Gusdon AM, Cheikhi A, Steer EK, Wang R, Baty C, Watkins S, Bahar I, Bayir H, Kagan VE. Cardiolipin externalization to the outer mitochondrial membrane acts as an elimination signal for mitophagy in neuronal cells. *Nat. Cell Biol.* 2013; 15:1197–1205. [PubMed: 24036476]
15. Goldmann O, Medina E. The expanding world of extracellular traps: Not only neutrophils but much more. *Front. Immunol.* 2013; 3:420. [PubMed: 23335924]
16. Dorio A, Cerella C, De Nicola M, D'Alessio M, Gualandi G, Ghibelli L. Non-apoptogenic Ca<sup>2+</sup>-related extrusion of mitochondria in anoxia/reoxygenation stress. *Ann. N. Y. Acad. Sci.* 2007; 1099:512–515. [PubMed: 17446495]
17. Nakajima A, Kurihara H, Yagita H, Okumura K, Nakano H. Mitochondrial extrusion through the cytoplasmic vacuoles during cell death. *J. Biol. Chem.* 2008; 283:24128–24135. [PubMed: 18593703]
18. Dalebroux ZD, Matamouros S, Whittington D, Bishop RE, Miller SI. PhoPQ regulates acidic glycerophospholipid content of the *Salmonella* Typhimurium outer membrane. *Proc. Natl. Acad. Sci. U.S.A.* 2014; 111:1963–1968. [PubMed: 24449881]
19. Zhang Q, Raouf M, Chen Y, Sumi Y, Sursal T, Junger W, Brohi K, Itagaki K, Hauser CJ. Circulating mitochondrial DAMPs cause inflammatory responses to injury. *Nature.* 2010; 464:104–107. [PubMed: 20203610]

20. Sims NR, Anderson MF. Isolation of mitochondria from rat brain using Percoll density gradient centrifugation. *Nat. Protoc.* 2008; 3:1228–1239. [PubMed: 18600228]
21. Kagan VE, Tyurin VA, Jiang J, Tyurina YY, Ritov VB, Amoscato AA, Osipov AN, Belikova NA, Kapralov AA, Kini V, Vlasova II, Zhao Q, Zou M, Di P, Svistunenko DA, Kurnikov IV, Borisenko GG. Cytochrome *c* acts as a cardiolipin oxygenase required for release of proapoptotic factors. *Nat. Chem. Biol.* 2005; 1:223–232. [PubMed: 16408039]
22. Tyurin VA, Balasubramanian K, Winnica D, Tyurina YY, Vikulina AS, He RR, Kapralov AA, Macphee CH, Kagan VE. Oxidatively modified phosphatidylserines on the surface of apoptotic cells are essential phagocytic ‘eat-me’ signals: Cleavage and inhibition of phagocytosis by Lp-PLA<sub>2</sub>. *Cell Death Differ.* 2014; 21:825–835. [PubMed: 24464221]
23. Losito I, Conte E, Introna B, Megli FM, Palmisano F. Improved specificity of cardiolipin peroxidation by soybean lipoxygenase: A liquid chromatography-electrospray ionization mass spectrometry investigation. *J. Mass Spectrom.* 2011; 46:1255–1262. [PubMed: 22223416]
24. Armengol C, Bartolí R, Sanjurjo L, Serra I, Amézaga N, Sala M, Sarrias MR. Role of scavenger receptors in the pathophysiology of chronic liver diseases. *Crit. Rev. Immunol.* 2013; 33:57–96. [PubMed: 23627007]
25. Peiser L, Gough PJ, Kodama T, Gordon S. Macrophage class A scavenger receptor-mediated phagocytosis of *Escherichia coli*: Role of cell heterogeneity microbial strain and culture conditions in vitro. *Infect. Immun.* 2000; 68:1953–1963. [PubMed: 10722588]
26. Baranova IN, Vishnyakova TG, Bocharov AV, Leelahavanichkul A, Kurlander R, Chen Z, Souza ACP, Yuen PST, Star RA, Csako G, Patterson AP, Eggerman TL. Class B scavenger receptor types I and II CD36 mediate bacterial recognition proinflammatory signaling induced by *Escherichia coli*, lipopolysaccharide and cytosolic chaperonin 60. *J. Immunol.* 2012; 188:1371–1380. [PubMed: 22205027]
27. Badeau RM, Metso J, Wähälä K, Tikkanen MJ, Jauhiainen M. Human macrophage cholesterol efflux potential is enhanced by HDL-associated 17 $\beta$ -estradiol fatty acyl esters. *J. Steroid Biochem. Mol. Biol.* 2009; 116:44–49. [PubMed: 19406243]
28. Zhao Y, Xiong Z, Lechner EJ, Klenotic PA, Hamburg BJ, Hulver M, Khare A, Oriss T, Mangalmurti N, Chan Y, Zhang Y, Ross MA, Stolz DB, Rosengart MR, Pilewski J, Ray P, Ray A, Silverstein RL, Lee JS. Thrombospondin-1 triggers macrophage IL-10 production and promotes resolution of experimental lung injury. *Mucosal Immunol.* 2014; 7:440–448. [PubMed: 24045574]
29. Pelegrin P, Barroso-Gutierrez C, Surprenant A. P2X<sub>7</sub> receptor differentially couples to distinct release pathways for IL-1 $\beta$  in mouse macrophage. *J. Immunol.* 2008; 180:7147–7157. [PubMed: 18490713]
30. Rossol M, Heine H, Meusch U, Quandt D, Klein C, Sweet MJ, Hauschildt S. LPS-induced cytokine production in human monocytes and macrophages. *Crit. Rev. Immunol.* 2011; 31:379–446. [PubMed: 22142165]
31. Stifano G, Affandi AJ, Mathes AL, Rice LM, Nakerakanti S, Nazari B, Lee J, Christmann RB, Lafyatis R. Chronic Toll-like receptor 4 stimulation in skin induces inflammation, macrophage activation, transforming growth factor beta signature gene expression, and fibrosis. *Arthritis Res. Ther.* 2014; 16:R136. [PubMed: 24984848]
32. Chesrown SE, Monnier J, Visner G, Nick HS. Regulation of inducible nitric oxide synthase mRNA levels by LPS INF- $\gamma$ , TGF- $\beta$  and IL-10 in murine macrophage cell lines and rat peritoneal macrophages. *Biochem. Biophys. Res. Commun.* 1994; 200:126–134. [PubMed: 7513155]
33. Martinez FO, Sica A, Mantovani A, Locati M. Macrophage activation and polarization. *Front. Biosci.* 2008; 13:453–461. [PubMed: 17981560]
34. Martinez FO, Gordon S. The M1 and M2 paradigm of macrophage activation: Time for reassessment. *F1000Prime Rep.* 2014; 6:13. [PubMed: 24669294]
35. Erdman LK, Cosio G, Helmers AJ, Gowda DC, Grinstein S, Kain KC. CD36 and TLR interactions in inflammation and phagocytosis: Implications for malaria. *J. Immunol.* 2009; 183:6452–6459. [PubMed: 19864601]
36. O’Neill LAJ, Bowie AG. The family of five: TIR-domain-containing adaptors in Toll-like receptor signalling. *Nat. Rev. Immunol.* 2007; 7:353–364. [PubMed: 17457343]

37. Perregaux DG, Gabel CA. Post-translational processing of murine IL-1: Evidence that ATP-induced release of IL-1 $\alpha$  and IL-1 $\beta$  occurs via a similar mechanism. *J. Immunol.* 1998; 160:2469–2477. [PubMed: 9498792]
38. Park BS, Song DH, Kim HM, Choi B-S, Lee H, Lee J-O. The structural basis of lipopolysaccharide recognition by the TLR4-MD-2 complex. *Nature.* 2009; 458:1191–1195. [PubMed: 19252480]
39. Kennedy MN, Mullen GE, Leifer CA, Lee C, Mazzoni A, Dileepan KN, Segal DM. A complex of soluble MD-2 and lipopolysaccharide serves as an activating ligand for Toll-like receptor 4. *J. Biol. Chem.* 2004; 279:34698–34704. [PubMed: 15175334]
40. Rolli J, Loukili N, Levrant S, Rosenblatt-Velin N, Rignault-Clerc S, Waeber B, Feihl F, Pacher P, Liaudet L. Bacterial flagellin elicits widespread innate immune defense mechanisms, apoptotic signaling, and a sepsis-like systemic inflammatory response in mice. *Crit. Care.* 2010; 14:R160. [PubMed: 20731882]
41. Scior T, Lozano-Aponte J, Figueroa-Vazquez V, Yunes-Rojas JA, Zähringer U, Alexander C. Three-dimensional mapping of differential amino acids of human, murine, canine and equine TLR4/MD-2 receptor complexes conferring endotoxic activation by lipid A, antagonism by Eritoran and species-dependent activities of lipid IVA in the mammalian LPS sensor system. *Comput. Struct. Biotechnol. J.* 2013; 7:e201305003. [PubMed: 24688739]
42. Underhill DM, Goodridge HS. Information processing during phagocytosis. *Nat. Rev. Immunol.* 2012; 12:492–502. [PubMed: 22699831]
43. Wu Y, Tibrewal N, Birge RB. Phosphatidylserine recognition by phagocytes: A view to a kill. *Trends Cell Biol.* 2006; 16:189–197. [PubMed: 16529932]
44. Maiti SN, Balasubramanian K, Ramoth JA, Schroit AJ.  $\beta$ -2-Glycoprotein 1-dependent macrophage uptake of apoptotic cells: Binding to lipoprotein receptor-related protein receptor family members. *J. Biol. Chem.* 2008; 283:3761–3766. [PubMed: 18073216]
45. Greenberg ME, Sun M, Zhang R, Febbraio M, Silverstein R, Hazen SL. Oxidized phosphatidylserine-CD36 interactions play an essential role in macrophage-dependent phagocytosis of apoptotic cells. *J. Exp. Med.* 2006; 203:2613–2625. [PubMed: 17101731]
46. Lee SJ, Evers S, Roeder D, Parlow AF, Risteli J, Risteli L, Lee YC, Feizi T, Langen H, Nussenzweig MC. Mannose receptor-mediated regulation of serum glycoprotein homeostasis. *Science.* 2002; 295:1898–1901. [PubMed: 11884756]
47. Gazi U, Martinez-Pomares L. Influence of the mannose receptor in host immune responses. *Immunobiology.* 2009; 214:554–561. [PubMed: 19162368]
48. Cox CC, Dougherty RW, Ganong BR, Bell RM, Niedel JE, Snyderman R. Differential stimulation of the respiratory burst and lysosomal enzyme secretion in human polymorphonuclear leukocytes by synthetic diacylglycerols. *J. Immunol.* 1986; 136:4611–4616. [PubMed: 3011896]
49. Li Y, Ye D. Molecular biology for formyl peptide receptors in human diseases. *J. Mol. Med.* 2013; 91:781–789. [PubMed: 23404331]
50. Sorice M, Circella A, Cristea IM, Garofalo T, Di Renzo L, Alessandri C, Valesini G, Esposti MD. Cardiolipin and its metabolites move from mitochondria to other cellular membranes during death receptor-mediated apoptosis. *Cell Death Differ.* 2004; 11:1133–1145. [PubMed: 15181455]
51. Rosenberger CM, Finlay BB. Phagocyte sabotage: Disruption of macrophage signalling by bacterial pathogens. *Nat. Rev. Mol. Cell Biol.* 2003; 4:385–396. [PubMed: 12728272]
52. Higa N, Toma C, Nohara T, Nakasone N, Takaesu G, Suzuki T. Lose the battle to win the war: Bacterial strategies for evading host inflammasome activation. *Trends Microbiol.* 2013; 21:342–349. [PubMed: 23712018]
53. Needham BD, Trent MS. Fortifying the barrier: The impact of lipid A remodelling on bacterial pathogenesis. *Nat. Rev. Microbiol.* 2013; 11:467–481. [PubMed: 23748343]
54. Canton J, Neculai D, Grinstein S. Scavenger receptors in homeostasis and immunity. *Nat. Rev. Immunol.* 2013; 13:621–634. [PubMed: 23928573]
55. Kim S, Elkon KB, Ma X. Transcriptional suppression of interleukin-12 gene expression following phagocytosis of apoptotic cells. *Immunity.* 2004; 21:643–653. [PubMed: 15539151]
56. Gutschmann T, Müller M, Carroll SF, MacKenzie RC, Wiese A, Seydel U. Dual role of lipopolysaccharide (LPS)-binding protein in neutralization of LPS and enhancement of LPS-

- induced activation of mononuclear cells. *Infect. Immun.* 2001; 69:6942–6950. [PubMed: 11598069]
57. Mueller M, Brandenburg K, Dedrick R, Schromm AB, Seydel U. Phospholipids inhibit lipopolysaccharide (LPS)-induced cell activation: A role for LPS-binding protein. *J. Immunol.* 2005; 174:1091–1096. [PubMed: 15634934]
  58. Lynn WA, Liu Y, Golenbock DT. Neither CD14 nor serum is absolutely necessary for activation of mononuclear phagocytes by bacterial lipopolysaccharide. *Infect. Immun.* 1993; 61:4452–4461. [PubMed: 7691750]
  59. Jungi TW, Sager H, Adler H, Brcic M, Pfister H. Serum factors cell membrane CD14 and  $\beta_2$  integrins are not required for activation of bovine macrophages by lipopolysaccharide. *Infect. Immun.* 1997; 65:3577–3584. [PubMed: 9284122]
  60. Esparza GA, Teghanemt A, Zhang D, Gioannini TL, Weiss JP. Endotoxin-albumin complexes transfer endotoxin monomers to MD-2 resulting in activation of TLR4. *Innate Immun.* 2012; 18:478–491. [PubMed: 21994253]
  61. Hashimoto M, Asai Y, Ogawa T. Treponemal phospholipids inhibit innate immune responses induced by pathogen-associated molecular patterns. *J. Biol. Chem.* 2003; 278:44205–44213. [PubMed: 12947124]
  62. Takasugi Y, Kurai F, Kazume I, Otsuka M, Negishi Y, Tada R, Aramaki Y. Down regulation of MyD88 in macrophages treated with liposomes composed of phosphatidylserine. *J. Pharm. Pharmacol.* 2013; 4:248–254.
  63. Mukundan L, Odegaard JI, Morel CR, Heredia JE, Mwangi JW, Ricardo-Gonzalez RR, Goh YPS, Eagle AR, Dunn SE, Awakuni JUH, Nguyen KD, Steinman L, Michie SA, Chawla A. PPAR- $\delta$  senses and orchestrates clearance of apoptotic cells to promote tolerance. *Nat. Med.* 2009; 15:1266–1272. [PubMed: 19838202]
  64. A-Gonzalez N, Bensinger SJ, Hong C, Beceiro S, Bradley MN, Zelcer N, Deniz J, Ramirez C, Diaz M, Gallardo G, de Galarreta CR, Salazar J, Lopez F, Edwards P, Parks J, Andujar M, Tontonoz P, Castrillo A. Apoptotic cells promote their own clearance and immune tolerance through activation of the nuclear receptor LXR. *Immunity.* 2009; 31:245–258. [PubMed: 19646905]
  65. Alam J, Kim YC, Choi Y. Potential role of bacterial infection in autoimmune diseases: A new aspect of molecular mimicry. *Immune Netw.* 2014; 14:7–13. [PubMed: 24605075]
  66. Root-Bernstein R, Fairweather D. Complexities in the relationship between infection and autoimmunity. *Curr. Allergy Asthma Rep.* 2014; 14:407. [PubMed: 24352912]
  67. Yang D, Oyaizu Y, Oyaizu H, Olsen GJ, Woese CR. Mitochondrial origins. *Proc. Natl. Acad. Sci. U.S.A.* 1985; 82:4443–4447. [PubMed: 3892535]
  68. Teghanemt A, Zhang D, Levis EN, Weiss JP, Gioannini TL. Molecular basis of reduced potency of underacylated endotoxins. *J. Immunol.* 2005; 175:4669–4676. [PubMed: 16177114]
  69. Matsuura M. Structural modifications of bacterial lipopolysaccharide that facilitate Gram-negative bacteria evasion of host innate immunity. *Front Immunol.* 2013; 4:109. [PubMed: 23745121]
  70. Olagnier D, Lavergne R-A, Meunier E, Lefèvre L, Dardenne C, Aubouy A, Benoit-Vical F, Ryffel B, Coste A, Berry A, Pipy B. Nrf2, a PPAR $\gamma$  alternative pathway to promote CD36 expression on inflammatory macrophages: Implication for malaria. *PLOS Pathog.* 2011; 7:e1002254. [PubMed: 21949655]
  71. Ballesteros I, Cuartero MI, Pradillo JM, de la Parra J, Pérez-Ruiz A, Corbí A, Ricote M, Hamilton JA, Sobrado M, Vivancos J, Nombela F, Lizasoain I, Moro MA. Rosiglitazone-induced CD36 up-regulation resolves inflammation by PPAR $\gamma$  and 5-LO-dependent pathways. *J. Leukoc. Biol.* 2014; 95:587–598. [PubMed: 24338629]
  72. Allavena P, Chieppa M, Monti P, Piemonti L. From pattern recognition receptor to regulator of homeostasis: The double-faced macrophage mannose receptor. *Crit. Rev. Immunol.* 2004; 24:179–192. [PubMed: 15482253]
  73. Liew FY, Xu D, Brint EK, O'Neill LAJ. Negative regulation of Toll-like receptor-mediated immune responses. *Nat. Rev. Immunol.* 2005; 5:446–458. [PubMed: 15928677]
  74. Kagan VE, Gleiss B, Tyurina YY, Tyurin VA, Elenström-Magnusson C, Liu S-X, Serinkan FB, Arroyo A, Chandra J, Orrenius S, Fadeel B. A role for oxidative stress in apoptosis: Oxidation and

- externalization of phosphatidylserine is required for macro-phage clearance of cells undergoing Fas-mediated apoptosis. *J. Immunol.* 2002; 169:487–499. [PubMed: 12077280]
75. Li K, Li Y, Shelton JM, Richardson JA, Spencer E, Chen ZJ, Wang X, Williams RS. Cytochrome c deficiency causes embryonic lethality and attenuates stress-induced apoptosis. *Cell.* 2000; 101:389–399. [PubMed: 10830166]
76. Folch J, Lees M, Sloan Estanley GH. A simple method for the isolation and purification of total lipides from animal tissues. *J. Biol. Chem.* 1957; 226:497–509. [PubMed: 13428781]
77. Farrera C, Fadeel B. Macrophage clearance of neutrophil extracellular traps is a silent process. *J. Immunol.* 2013; 191:2647–2656. [PubMed: 23904163]
78. Hanwell MD, Curtis DE, Lonie DC, Vandermeersch T, Zurek E, Hutchison GR. Avogadro: An advanced semantic chemical editor, visualization, and analysis platform. *J. Cheminform.* 2012; 4:17. [PubMed: 22889332]
79. Ohto U, Fukase K, Miyake K, Shimizu T. Structural basis of species-specific endotoxin sensing by innate immune receptor TLR4/MD-2. *Proc. Natl. Acad. Sci. U.S.A.* 2012; 109:7421–7426. [PubMed: 22532668]
80. Trott O, Olson AJ. AutoDock Vina: Improving the speed accuracy of docking with a new scoring function, efficient optimization and multithreading. *J. Comput. Chem.* 2010; 31:455–461. [PubMed: 19499576]
81. Sanner MF. Python: A programming language for software integration and development. *J. Mol. Graph. Model.* 1999; 17:57–61. [PubMed: 10660911]

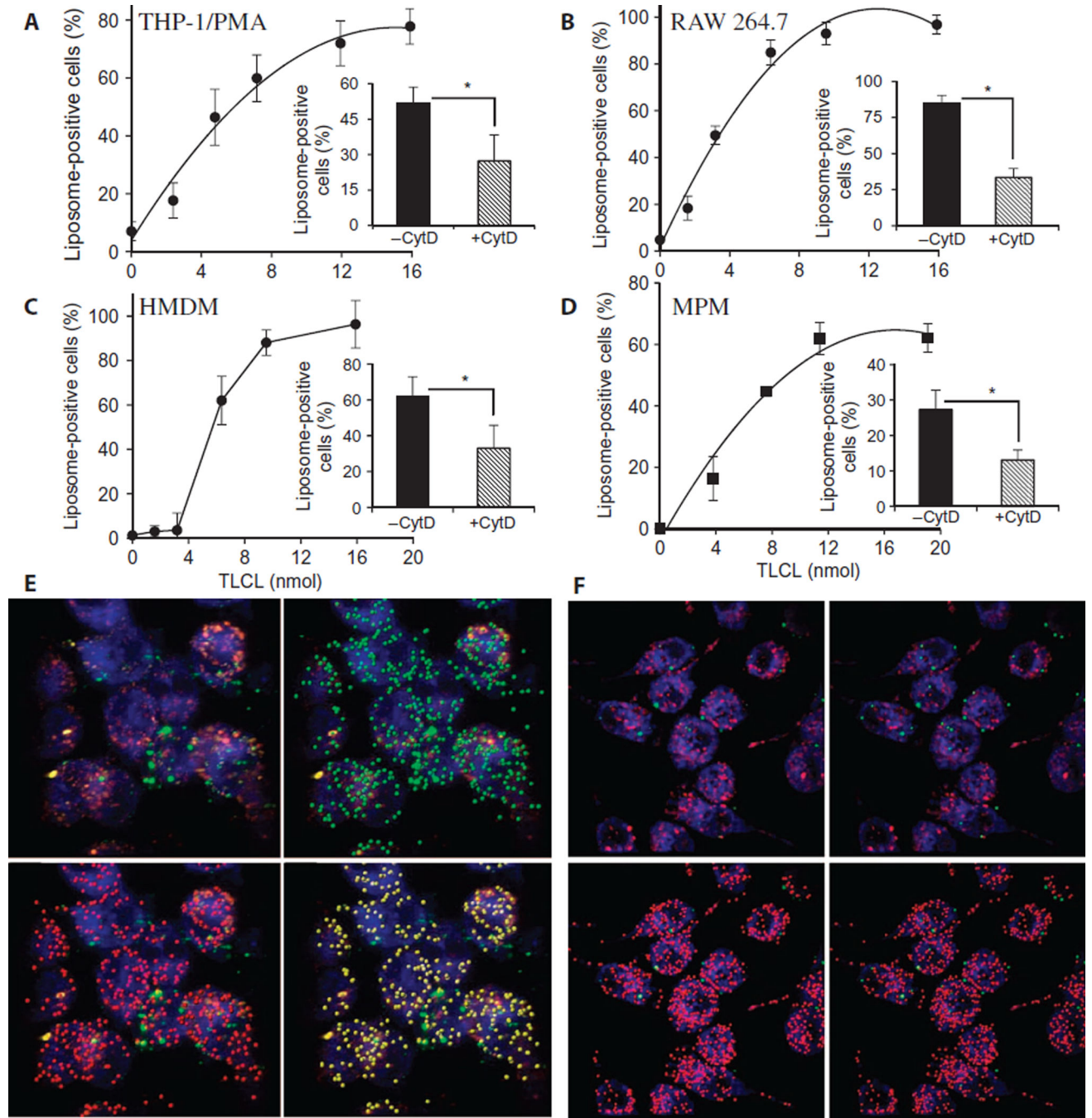


**Fig. 1. Macrophages phagocytose CL-containing liposomes**

(A to D) The indicated macrophages and macrophage-like cell lines were incubated for 60 min with fluorescent liposomes composed of increasing amounts of TLCL in PC. The cells were then washed, trypsinized, and assessed for their phagocytosis of the liposomes by flow cytometry. Data are means  $\pm$  SD of three to five experiments and are expressed as the percentage of macrophages that phagocytosed the liposomes. Insets: The indicated cells were incubated for 60 min with liposomes (5 nmol of TLCL) in the absence or presence of 20  $\mu$ M CytD before being assessed for phagocytosis. Data are means  $\pm$  SD of three to five

experiments.  $*P < 0.05$  by  $t$  test. **(E and F)** RAW 264.7 cells incubated for 20 min with fluorescent liposomes composed of NBD (7-nitro-2-1,3-benzoxadiazol-4-yl)-CL (green) (E) or NBD-PC (green) (F) were loaded with LysoTracker Deep Red (red) and ER-Tracker Blue-White (blue). Images were captured and analyzed as described in Materials and Methods. The lysosomal and NBD signals were segmented, and the degree of colocalization was calculated. Top left: Maximal intensity projection of the cells after incubation with NBD-CL (E) or NBD-PC (F). Top right: The segmented NBD signals are shown as bright green spots. Bottom left: The segmented lysosomes are shown as bright red spots. Bottom right: Colocalized lysosomes and NBD signals appear as yellow spots. The degree of colocalization in (E) was 85%, whereas there was no statistically significant degree of colocalization in (F). Images in (E) and (F) are representative of three experiments.

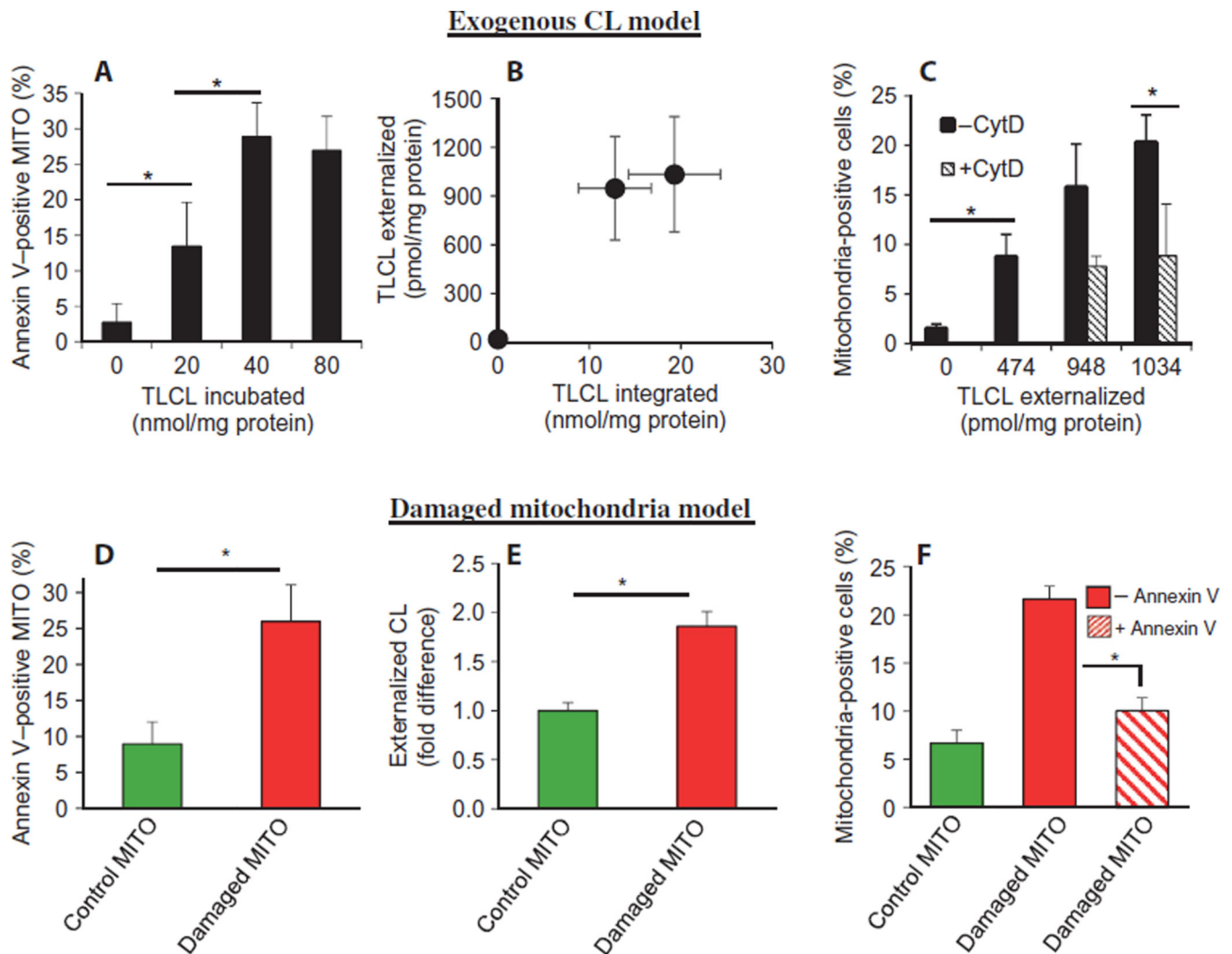


**Fig. 2. Mitochondria that present CL on their surface are engulfed by macrophages**  
 (A) Semiquantitative analysis of the amounts of externalized TLCL on the surface of mitochondria (MITO) after incubation with the indicated concentrations of TLCL was performed by flow cytometric analysis with FITC-conjugated annexin V in the presence of 200  $\mu\text{M}$   $\text{Ca}^{2+}$ . Data are presented as the percentages of mitochondria that were annexin V-positive and are means  $\pm$  SD of three experiments. \* $P < 0.05$  by  $t$  test. (B) Quantification of the amount of TLCL presented on the mitochondrial surface was performed by incubating mitochondria with  $\text{PLA}_2$  under nonpermeable conditions and then subjecting the extracted lipids to LC-MS analysis to detect mono-lyso-CL. Numbers on the  $x$  axis represent the amount of TLCL integrated into the mitochondria (as determined by LC-MS analysis; fig. S3, A to C). Data are means  $\pm$  SD of the amounts of TLCL on the mitochondrial surface from three experiments. (C) RAW 264.7 cells were left untreated or were pretreated with 20  $\mu\text{M}$  CytD before being incubated with MitoTracker Red-labeled, TLCL-presenting mitochondria. The cells were washed and trypsinized, and the extent of their phagocytosis of the mitochondria was assessed by flow cytometric analysis. Data are means  $\pm$  SD of three to five experiments. \* $P < 0.05$  by  $t$  test. (D to F) MitoTracker Red-labeled mitochondria (P2

fraction) isolated from control and ActD-treated (Damaged) MEFs were assessed for CL externalization by flow cytometric analysis with annexin V-FITC (D) and PLA<sub>2</sub> treatment (E). (F) RAW 264.7 cells were incubated with the mitochondria described in (D), and the extent to which they phagocytosed the mitochondria was determined as described for (C). Data in (D) to (F) are means  $\pm$  SD of three experiments. \* $P < 0.05$  by *t* test.

Author Manuscript

Author Manuscript

Author Manuscript

Author Manuscript

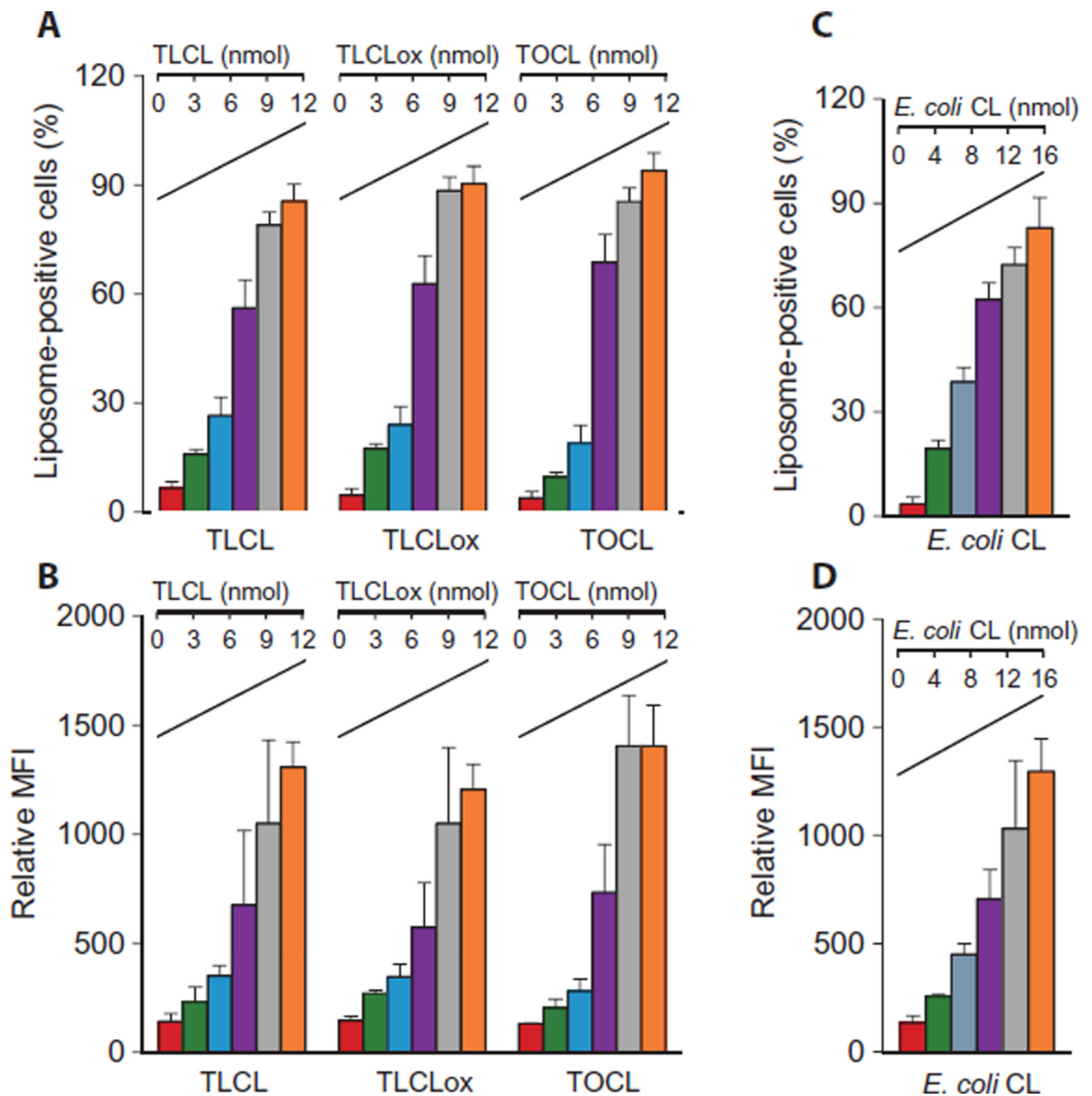


**Fig. 3. Acyl chain composition does not affect the phagocytosis of CL-containing liposomes** (A to D) RAW 264.7 cells were incubated for 60 min with liposomes composed of 0 to 12 nmol of TLCL, peroxidized TLCL (TLCLox), or TOCL (A and B) or 0 to 16 nmol of *E. coli* CL (C and D) as shown by the trace line. The cells were then washed, trypsinized, and analyzed by flow cytometry to assess their ability to phagocytose the liposomes. Data are presented as the percentage of liposome-positive cells (A and C) and the relative mean fluorescence intensity (MFI) of FITC (B and D). Data are means  $\pm$  SD of three to five experiments.

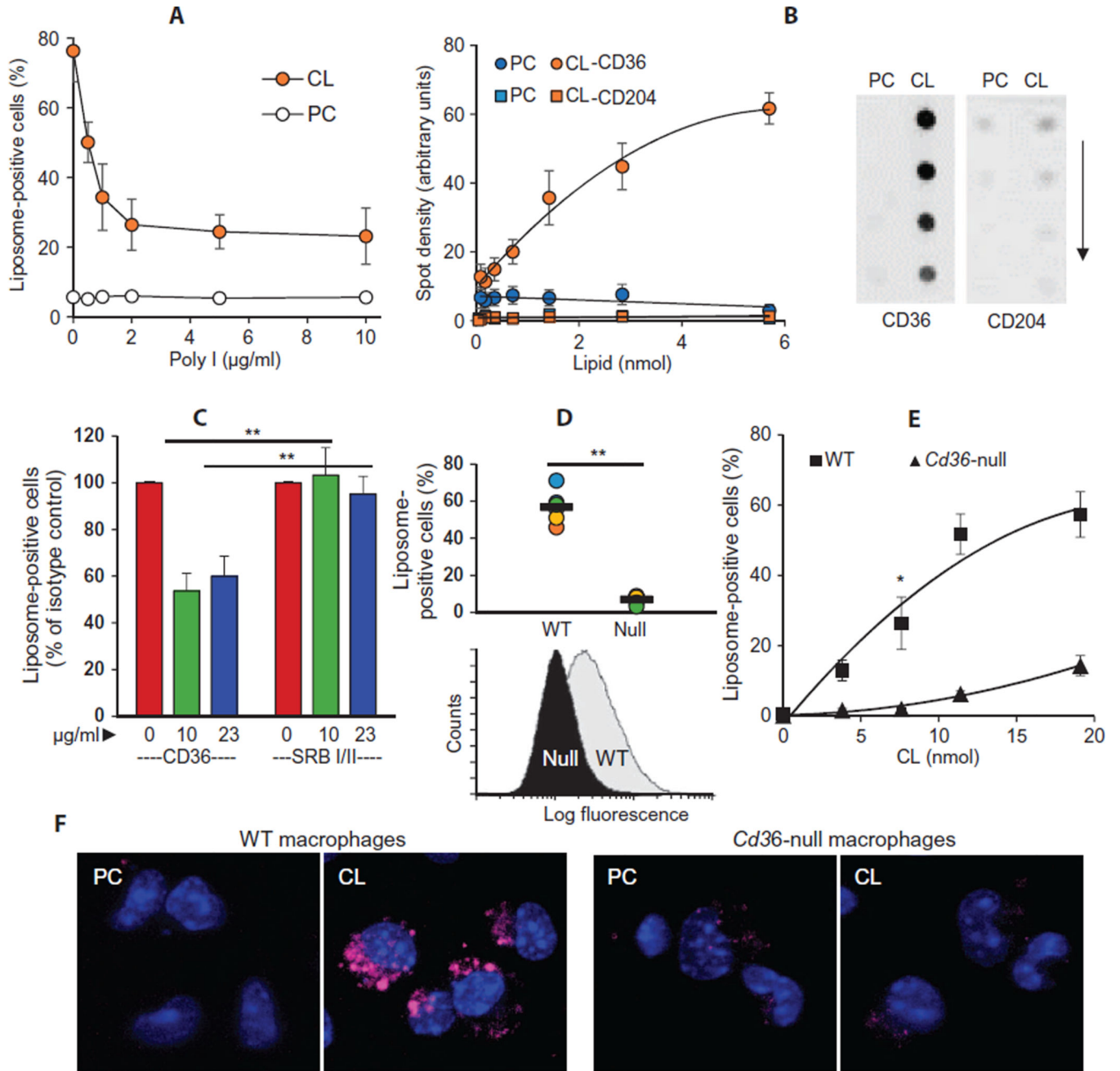


**Fig. 4. CL-dependent phagocytosis requires the SR CD36**

(A) RAW 264.7 cells were incubated with TLCL-liposomes (12 nmol, CL) in the absence or presence of Poly I. The macrophages were then washed, trypsinized, and assessed for phagocytosis by flow cytometry. PC-liposomes were used as a control. Data are means  $\pm$  SD of four experiments. (B) Left: Serial dilutions of PC or TLCL (CL) immobilized on polyvinylidene difluoride (PVDF) membranes were incubated with His-tagged recombinant proteins corresponding to the extracellular domains of CD36 (circles) or CD204 (squares). Binding was visualized with horseradish peroxidase (HRP)-conjugated anti-His tag antibodies. Data are means  $\pm$  SD of three experiments. Right: Representative lipid blots

incubated with the recombinant CD36 or CD204 proteins. The direction of the serial dilutions of phospholipid is denoted by the arrow. Blots are representative of three experiments. (C) RAW 264.7 cells were incubated with TLCL-liposomes (12 nmol, CL) in the absence or presence of the indicated concentrations of anti-CD36 or anti-SRB I/II blocking antibodies or their respective isotype controls. The cells were then analyzed by flow cytometry to assess phagocytosis. Data are presented as the percentage of antibody-treated cells that were positive for liposomes relative to the percentage of isotype control-treated cells that were positive for liposomes. Data are means  $\pm$  SD of three experiments.  $**P < 0.01$  by *t* test. (D to F) MPMs isolated from thioglycollate-treated wild-type (WT) mice and *Cd36*<sup>-/-</sup> (Null) mice were assessed for their ability to phagocytose fluorescent N-NBD-phosphatidylethanolamine (N-NBD-PE)-labeled liposomes (38 nmol of total lipid) composed of PC alone or TLCL (11.4 nmol, CL) in PC. (D) Top: Each circle represents data from MPMs isolated from a single mouse. The black horizontal bars show the mean values. Data are means  $\pm$  SD of six experiments.  $**P < 0.01$  by *t* test. Bottom: Representative flow cytometry histogram. (E) Flow cytometric analysis of the phagocytosis of liposomes containing the indicated amounts of TLCL (CL) by WT and *Cd36*<sup>-/-</sup> MPMs. Data are means  $\pm$  SD of three experiments.  $*P < 0.05$  by *t* test. (F) RAW 264.7 cells were incubated for 20 min with fluorescent 1,1'-dioctadecyl-3,3,3',3'-tetramethylindocarbocyanine perchlorate (DiI)-labeled liposomes (red, 38 nmol of total lipid) composed of PC alone or TLCL (11.4 nmol, CL) in PC. The cells were then washed, fixed, stained with 4',6-diamidino-2-phenylindole (DAPI) (blue), and imaged. Data are representative confocal projection snapshots from three experiments.

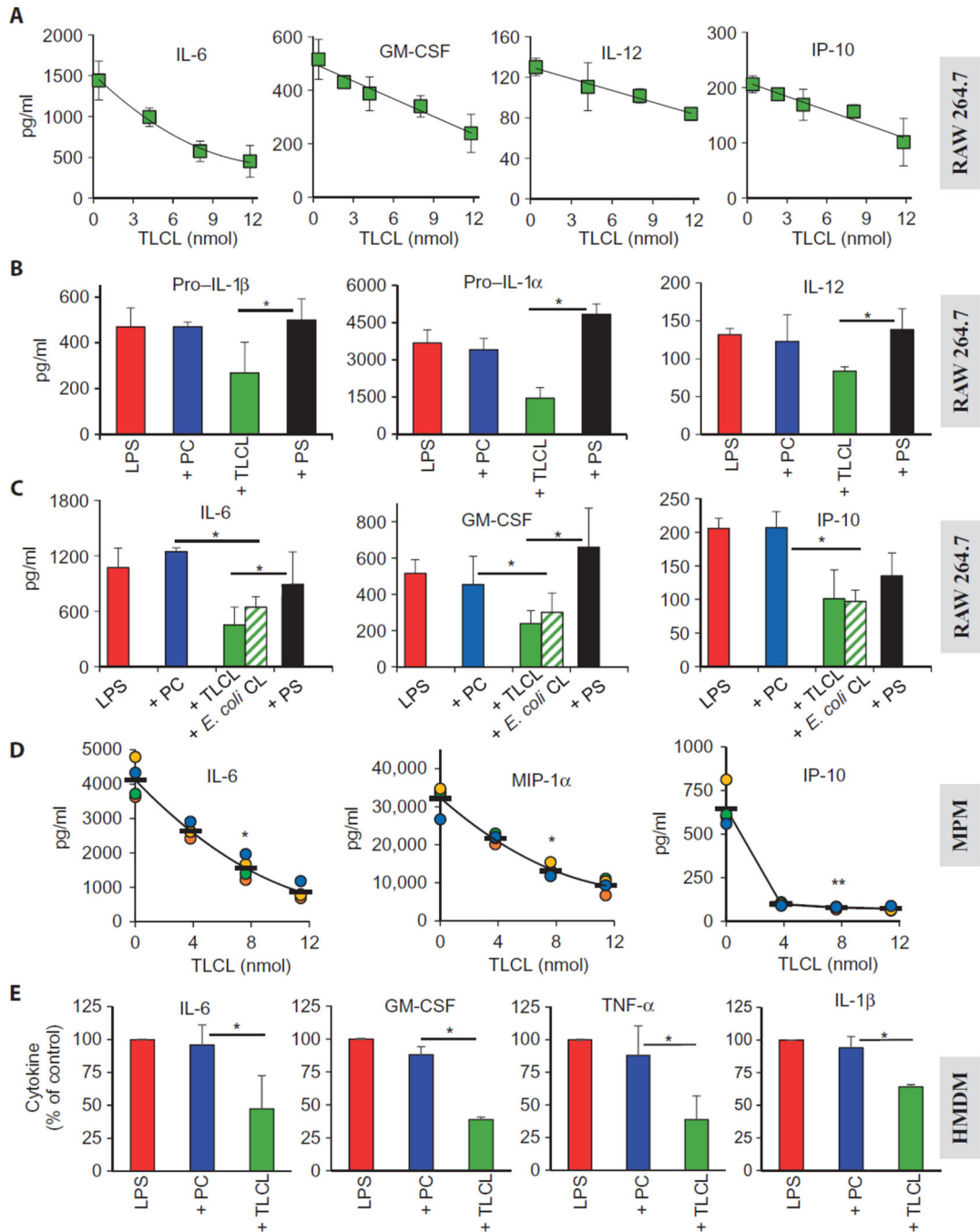


**Fig. 5. CL inhibits the LPS-dependent production of inflammatory cytokines**

(A to C) RAW 264.7 cells were incubated for 16 hours with LPS alone, with LPS in the presence of liposomes (38 nmol of total lipid) composed of the indicated amounts of TLCL (A), or with LPS in the presence of liposomes (38 nmol of total lipid) composed of PC alone, TLCL, or *E. coli* CL or PS (11.4 nmol of lipid) in PC (B and C). Culture media or cell lysates (for pro-IL-1 $\alpha$  and pro-IL-1 $\beta$ ) were analyzed for the indicated cytokines by Luminex assay. Data are means  $\pm$  SD of three experiments. \* $P$  < 0.05 by  $t$  test. (D) MPMs were incubated with LPS alone or in the presence of liposomes (38 nmol of total lipid)

containing the indicated amounts of TLCL in PC. The amounts of the indicated cytokines secreted in the cell culture medium were determined by Luminex assay. Each circle represents data from MPMs isolated from a single mouse. The black horizontal bars denote means. Data are means  $\pm$  SD of four experiments. \* $P < 0.05$ , \*\* $P < 0.01$  by  $t$  test. (E) HMDMs from healthy donors were incubated for 16 hours with LPS alone or with LPS in the presence of PC-liposomes or TLCL-liposomes (11.4 nmol of CL). Cell culture media were then analyzed by Luminex assay to determine the amounts of the indicated cytokines. Data are presented as a percentage of the amount of the indicated cytokines secreted by cells treated with LPS alone. Data are means  $\pm$  SD of three experiments. \* $P < 0.05$  by  $t$  test. MIP-1 $\alpha$ , macrophage inflammatory protein-1 $\alpha$  (also known as CCL3); TNF- $\alpha$ , tumor necrosis factor- $\alpha$ .

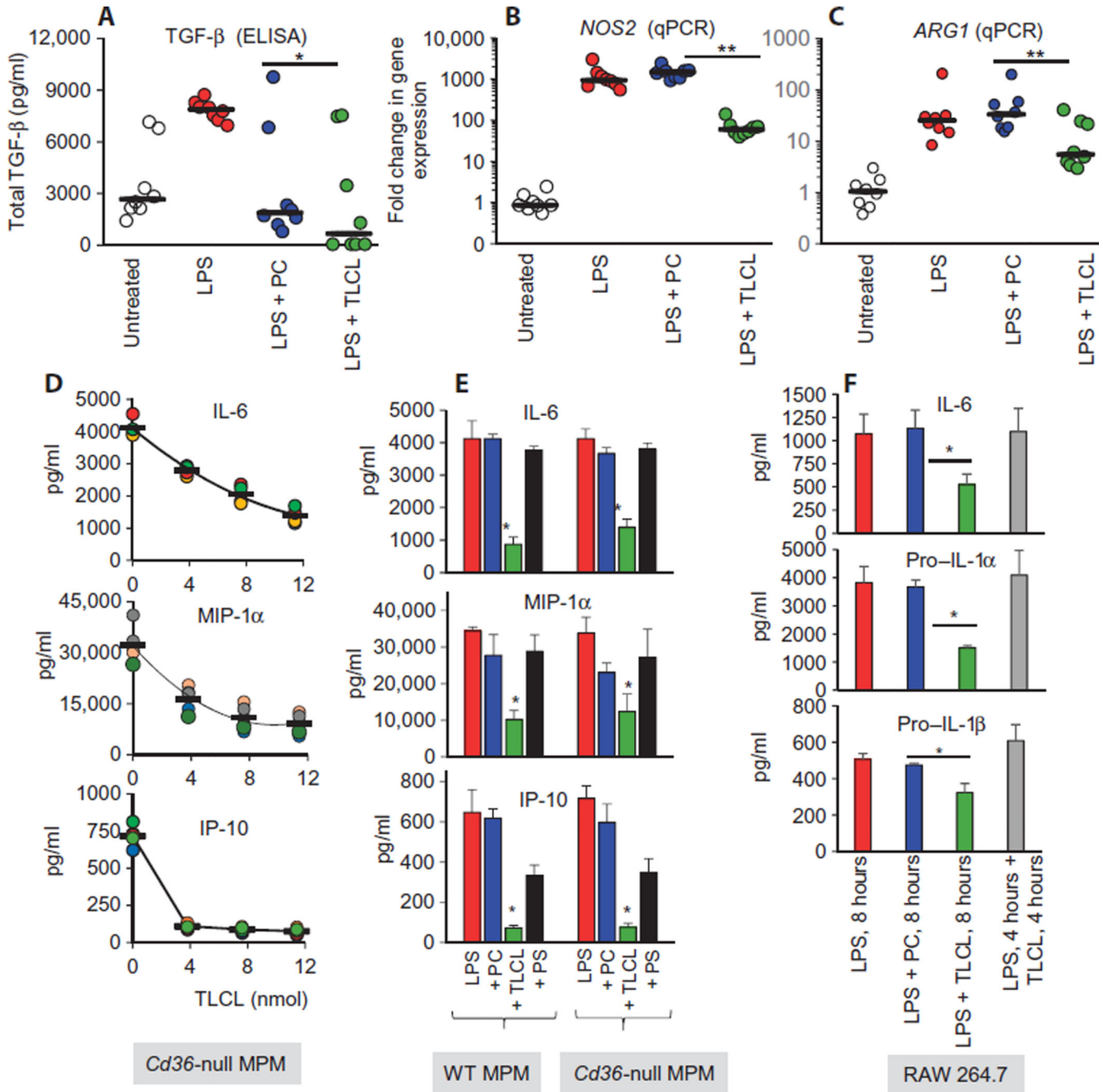


**Fig. 6. CL inhibits the expression of genes encoding inflammatory and anti-inflammatory factors and block LPS signaling through a CD36-independent mechanism**

(A) MPMs from C57BL/6J mice (eight mice) were plated in six-well plates and were left untreated or were incubated for 16 hours with LPS alone or with LPS in the presence of PC-liposomes or TLCL-liposomes (11.4 nmol of TLCL). Cell culture media were analyzed by ELISA to determine the amounts of TGF- $\beta$  secreted by the cells. Each circle represents data from MPMs isolated from a single mouse. Black horizontal bars denote median values. Data were analyzed with a nonparametric Friedman's test, which indicated that LPS and both liposome treatments had differential effects [ $\chi^2_{(3,n=8)} = 13.4, P < 0.01$ ] on TGF- $\beta$  secretion.

Follow-up pairwise comparisons with Bonferonni corrected level of observed significance showed that TLCL-liposomes significantly inhibited the LPS-dependent production of TGF- $\beta$  (median, 683.3 versus 7893.3;  $P < 0.01$ ). Although a difference in the median TGF- $\beta$  production was also observed between cells treated with LPS alone and those co-incubated with LPS and PC-liposomes (median, 1886.9), it did not reach the same level of statistical significance ( $P = 0.072$ ). **(B and C)** MPMs were incubated as described for **(A)**, after which their RNA was extracted as described in Materials and Methods. The RNA samples were analyzed by qPCR to determine the relative abundances of *NOS2* mRNA **(B)** and *ARG1* mRNA **(C)** normalized to that of 18S rRNA. Data were analyzed with a nonparametric Friedman's test. Black horizontal bars denote medians.  $**P < 0.001$  based on a nonparametric Friedman's test with Bonferroni correction. Each circle represents data from MPMs isolated from a single mouse. **(D and E)** MPMs from *Cd36*<sup>-/-</sup> mice **(D and E)** and WT mice **(E)** were incubated for 16 hours with LPS alone or in the presence of liposomes composed of the indicated amounts of TLCL **(D)** or in the presence of PC-liposomes, TLCL-liposomes (11.4 nmol), or PS-liposomes (11.4 nmol) **(E)**. Cell culture media were then analyzed by Luminex assay to determine the concentrations of the indicated cytokines. Each circle in **(D)** represents data from MPMs isolated from a single mouse. Black horizontal bars denote means. Data are means  $\pm$  SD of four experiments. Data in **(E)** are means  $\pm$  SD of four mice.  $*P < 0.05$  by *t* test. **(F)** RAW 264.7 cells were treated for 8 hours with LPS alone, for 8 hours with LPS together with the indicated liposomes, or for 4 hours with LPS followed by 4 hours of incubation with CL-liposomes. Cell culture media or lysates (for pro-IL-1 measurement) were then analyzed by Luminex assay to determine the concentrations of the indicated cytokines. Data are means  $\pm$  SD of three experiments.  $*P < 0.05$  by *t* test.

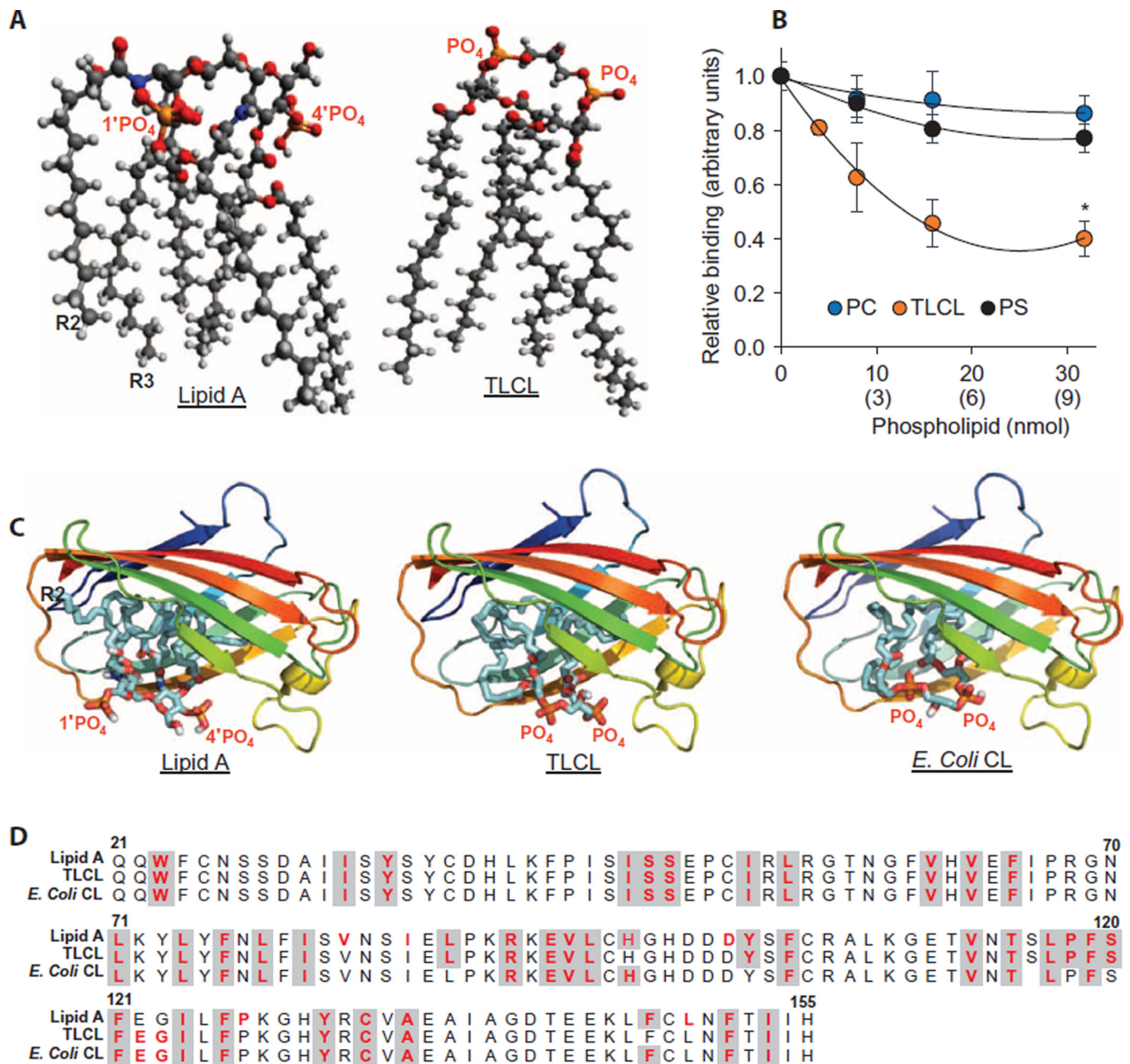


**Fig. 7. CL competes with LPS for binding to the TLR4 co-receptor MD2**

(A) Structures of lipid A and TLCL were generated by Avogadro software with structural data obtained from the LIPID MAPS Lipidomics Gateway. (B) ELISA plates containing immobilized recombinant MD2 protein (50 ng) were blocked with ovalbumin and then incubated for 90 min with biotinylated LPS (50 ng) in the absence or presence of PC-liposomes, TLCL-liposomes, or PS-liposomes. The plates were washed and then incubated for 60 min with HRP-conjugated streptavidin to visualize bound biotinylated LPS by TMB (3,3',5,5'-tetramethylbenzidine)-ELISA. Numbers on the x axis refer to the total amounts of phospholipids, whereas the numbers in parentheses refer specifically to the amounts of TLCL or PS. Data are means  $\pm$  SD of three experiments. \* $P < 0.05$  by  $t$  test. (C) Lipid A,

TLCL, and *E. coli* CL (17:1/15:0/16:0/18:1-CL is shown) were docked to the crystal structure of MD2 with AutoDock Vina software (<http://vina.scripps.edu>). The binding poses of the top-ranked models are shown. MD2, cartoon representation with spectral colors. Blue represents the N terminus, and red represents the C terminus. For lipids: cyan, acyl chains; blue, nitrogen; red, oxygen; orange, phosphorus. **(D)** The amino acid residues of MD2 that were identified to interact with lipid A, TLCL, and *E. coli* CL from the molecular docking models presented in (C) are shown in red. Gray boxes denote those interacting amino acid residues that are common to lipid A and the CLs.

Author Manuscript

Author Manuscript

Author Manuscript

Author Manuscript